



New insights in the relation between climate and slope failures at high-elevation sites

Roberta Paranunzio^{1,2} · Marta Chiarle² · Francesco Laio³ · Guido Nigrelli² · Laura Turconi² · Fabio Luino²

Received: 16 March 2018 / Accepted: 13 October 2018 / Published online: 13 November 2018
© Springer-Verlag GmbH Austria, part of Springer Nature 2018

Abstract

Climate change is now unequivocal; however, the type and extent of terrestrial impacts are still widely debated. Among these, the effects on slope stability are receiving a growing attention in recent years, both as terrestrial indicators of climate change and implications for hazard assessment. High-elevation areas are particularly suitable for these studies, because of the presence of the cryosphere, which is particularly sensitive to climate. In this paper, we analyze 358 slope failures which occurred in the Italian Alps in the period 2000–2016, at an elevation above 1500 m a.s.l. We use a statistical-based method to detect climate anomalies associated with the occurrence of slope failures, with the aim to catch an eventual climate signal in the preparation and/or triggering of the considered case studies. We first analyze the probability values assumed by 25 climate variables on the occasion of a slope-failure occurrence. We then perform a dimensionality reduction procedure and come out with a set of four most significant and representative climate variables, in particular heavy precipitation and short-term high temperature. Our study highlights that slope failures occur in association with one or more climate anomalies in almost 92% of our case studies. One or more temperature anomalies are detected in association with most case studies, in combination or not with precipitation (47% and 38%, respectively). Summer events prevail, and an increasing role of positive temperature anomalies from spring to winter, and with elevation and failure size, emerges. While not providing a final evidence of the role of climate warming on slope instability increase at high elevation in recent years, the results of our study strengthen this hypothesis, calling for more extensive and in-depth studies on the subject.

1 Introduction

The effects of climate change on natural systems are the object of worldwide debate, in both science and policy. According to the Fifth Assessment Report of the Intergovernmental Panel on Climate Change (Team et al. 2014), an average global increase of about 0.85 °C in land and ocean surface temperature has been recorded over the period 1880–2012 (Team et al. 2014). At the global scale, the first decade of the twenty-first century has been the warmest one since 1850 and 2016 resulted to be

the warmest year on record globally (Northon 2017); further warming (in the range of 0.3–0.7 °C between 2016 and 2030) is expected based on climate projections (Gobiet et al. 2014). Changes in extreme weather events, as a rise in high extreme temperatures and a decrease in low ones, have been observed since 1950 almost worldwide (Stocker et al. 2013). Changes in precipitation have also been observed, but confidence is lower, since an evident signal has not been detected worldwide, also because precipitation features at a site are more sensitive than temperature to the orographic and physiographic characteristics of the local territory (Brunetti et al. 2009).

If climate change is unequivocal, the full understanding of its impact on natural environments poses further challenges, due to the inherent complexity of these systems. In this framework, the cryosphere is considered a “*natural thermometer*” (Stocker et al. 2013) of climate change (in particular global warming, Käab et al. 2007), due to its sensitivity to change in climate variables. Studies on high-elevation/latitude areas show an overall framework of ice degradation at global and regional scales in response to air temperature increase (Zemp et al. 2015; Chadburn et al. 2017). In high-mountain areas, cryosphere degradation, and in particular glacier shrinkage, permafrost thawing, and spring snowpack decreasing, have,

Electronic supplementary material The online version of this article (<https://doi.org/10.1007/s00704-018-2673-4>) contains supplementary material, which is available to authorized users.

✉ Roberta Paranunzio
roberta.paranunzio@ucc.ie

- ¹ Present address: Centre for Maritime and Renewable Energy - MaREI Centre, Beaufort Building – ERI, University College Cork, Ringaskiddy, Co. Cork, Ireland
- ² Consiglio Nazionale delle Ricerche – Istituto di Ricerca per la Protezione Idrogeologica (IRPI), Torino, Italy
- ³ Politecnico di Torino, Torino, Italy

as direct consequence, the worsening of the mechanical conditions of rocks and soils (Fischer et al. 2006). One of the main consequences is slope destabilization (Gruber and Haeberli 2007; Harris et al. 2009), with shear strength reduction (Davies et al. 2001), opening of deep thaw joints, fracture displacement, and change in the stress field (Weber et al. 2017) acting as the triggers in a context of climate warming. Several studies, in fact, confirm an overall growing trend of slope instability worldwide (Huggel et al. 2010).

The European Alpine Region represents a key research hotspot for natural hazards studies, because of its complex climatic, geologic and physiographic setting, and the high touristic value of the entire area (Beniston et al. 2018; Haeberli et al. 2015). Studies on mass-wasting processes have gained an increasing attention in recent years, and a growing number of events is documented in glacial and periglacial areas, in particular since the hot summer of 2003 (Ravelin et al. 2017). The number of events of slope instability is expected to increase in the next future, even if several studies indicate a more complex response of slope stability to climate change (Gariano and Guzzetti 2016; Stoffel and Huggel 2017).

Among the different factors affecting slope stability, attention is here devoted to precipitation and temperature. Precipitation is known as a main driver of landslides in various geomorphological settings including the European (Italian) Alps (Peruccacci et al. 2017; Palladino et al. 2018). Changes in rainfall duration and intensity, combined with higher temperature, are supposed to enhance mass-wasting processes in high mountains, in particular those driven by water as debris and mudflows (Rebetz et al. 1997; Chiarle et al. 2011; Pavlova et al. 2014). The combination of abundant precipitation (rainfall and snowfall) and higher temperature is supposed to have a role in initiating shallow landslides (Saez et al. 2013) at high altitude as well. The effect of air temperature variations on rock and ice stability is even more complex to understand (Nigrelli et al. 2018). For example, in the Monte Rosa massif, Huggel et al. (2010) relate air temperature increase to various rock/ice avalanches and debris flows, occurred in the area in recent years. Recent studies relate the increased trend of rockfall activity affecting high-alpine steep rock walls to anomalies in mean temperatures in the hottest period of the year (Ravelin and Deline 2015), whereas other papers focus on changes in high daily extremes temperature potentially causing rockfalls over the European Alps (Allen and Huggel 2013). Other works highlight the role of summer heatwaves in the increased slope-failure activity on permafrost affected rock walls in the European Alps (Ravelin et al. 2017). Thus, the linkage between climate and slope failures at high elevation is definitely difficult to investigate, and many authors have pointed out the diffuse lack of shared and standardized strategies to face the problem (GAPHAZ 2017).

Assessing how climate variables could effectively influence slope-failure initiation and/or preparation mechanisms

is crucial in this framework (Huggel et al. 2013). Paranunzio et al. (2015) have proposed a statistical-based approach to detect anomalous values in the climate variables at the date of a slope failure, with application on five slope instability events of different types, occurred in glacial and periglacial areas of the Piedmont Alps (Northwestern Italy). The role of air temperature anomalies as the main trigger has been clearly spotted. To further investigate the role of air temperature variations at high-elevation sites, Paranunzio et al. (2016) analyzed 41 rock falls in the Italian Alps from 1997 to 2013, again demonstrating that the majority of slope instability events can indeed be associated to air temperature anomalies. However, the limited size of the considered dataset did not allow to fully disentangle the relations between climate change and slope instability.

In the present work, we aim to catch a possible climate signal behind the preparation and/or triggering of slope instability processes in high-mountain areas starting from a robust sample of more than 400 events occurred above 1500 m a.s.l. in the Italian Alps from year 2000 on. By performing this analysis, we aim to address the following research questions:

- i. Can temperature and precipitation be considered as key conditioning and/or triggering factors for slope failures at high-elevation sites? What climate variables are most relevant for slope instability?
- ii. How can the climate signal detected be linked to the process typology and to its spatiotemporal distribution?
- iii. Can climate change be deemed responsible for the observed increasing trend of slope instability at high elevation? What can be expected in the future?

The paper is organized as follows. After a brief description of the general setting of the study, we describe how we constructed the inventory and list the climate data used. This is followed by an explanation of the procedure for data preparation and validation and by a step-by-step description of the methodological approach. Finally, the main results are described and discussed, presenting a critical analysis of the major outcomes, of the unresolved questions and of the possible further steps.

2 Study area

We focus on the entire Alpine Italian region, stretching 1200 km from E to W and covering about 5200 km², i.e., 27.3% of the European Alps. The study area extends from 6° to 13° E and from 44° to 47° N, from the Mediterranean Sea (Franco-Italian border) stretching eastward to Slovenia (Fig. 1).

The Alpine chain developed from the subduction of a Mesozoic ocean and the collision between the Adriatic (Austroalpine-Southalpine) and European (Penninic-

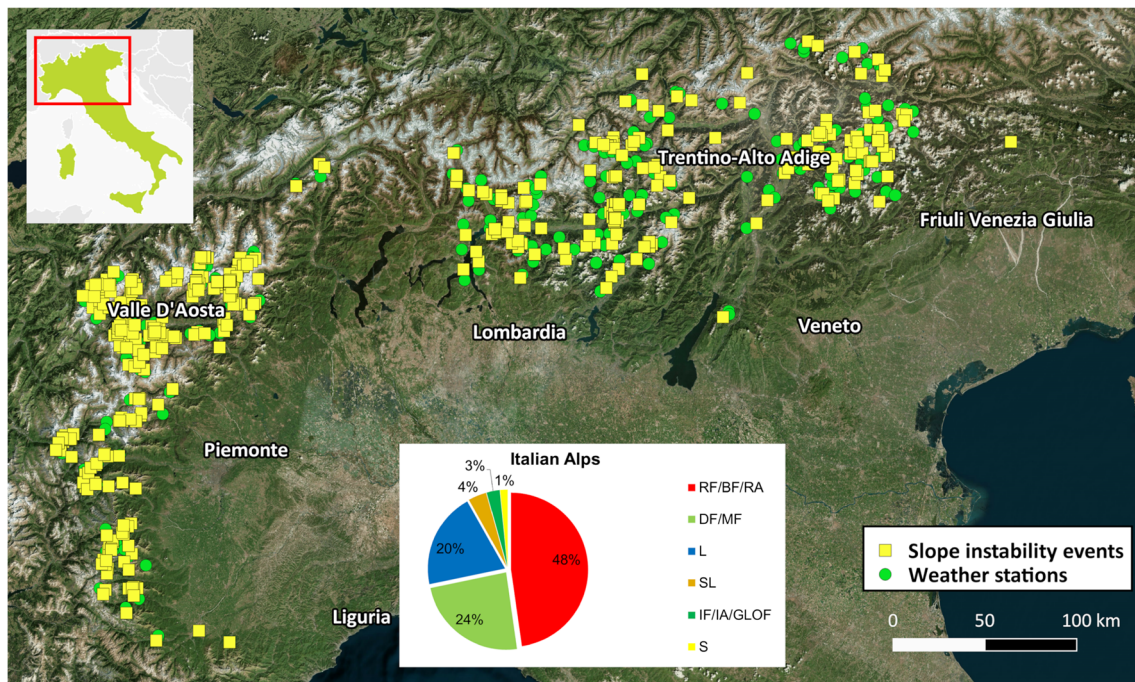


Fig. 1 Map showing 401 slope instability events included in the catalog (squares) and 131 weather stations used in this work (dots); type and sample size of the instability processes included in the catalog are

represented in the white box; RF, rockfall; BF blockfall; RA, rock avalanche; DF, debris flow; MF, mudflow; L, landslide; SL, slide; IF, ice fall; IA, ice avalanche; GLOF, glacial lake outburst flood; S, (soil) slip

Helvetic) continental margins (Dal Piaz et al. 2003). As a result, the Alps may be distinguished into two belts, separated by the Periadriatic (Insubric) lineament, which are characterized by an opposite direction of tectonic transport and have a different size, age, and geological history. The Europe-vergent belt is a thick collisional wedge, dating back to Cretaceous-Neogene and composed of continental and minor oceanic units. The Southern Alps is a minor, non-metamorphic, Neogene belt, displaced to the south. This complex geological history is at the base of the amazing geodiversity of the Alps, which culminates with the Mont Blanc Massif (4810 m a.s.l.), on the Western side. After their formation, the Alps have been sculptured by glaciers, running waters and slope failures, to reach their present configuration. Both the geologic and morphologic setting strongly influence the proneness of slopes to failure. The last important glacier advance (Little Ice Age) ended around 1850: since then, European glaciers suffered a strong area reduction of approximately 50% (Zemp et al. 2015). Due to the specific topoclimatic and physiographic setting, glacier shrinkage has been particularly marked on the Italian side of the Alps, up to the almost complete disappearance at the lower altitudes and latitudes (Nigrelli et al. 2014). Present glaciers (Salvatore et al. 2015; Smiraglia et al. 2015) are mainly located in the Valle d'Aosta region (36% of the total glacierized Italian area), followed by Trentino Alto Adige (31%), Lombardia (24%), Piemonte (8%), and Veneto (1%). Permafrost distribution in the Alps is highly complex and affected by a huge spatial variability,

mainly due to topographic effects (Harris et al. 2009). Studies carried out on the European Alps have found evidence of permafrost approximately since 2600 m a.s.l., but it can be found at 3500 m a.s.l. in unfavorable conditions, as south-facing rock walls (Cremonese et al. 2011).

The complex topographical and geographical context influences the climate of the Greater Alpine Region (HISTALP 2018), which is characterized by a high spatial variability of precipitation and temperature patterns at regional and local scales (Auer et al. 2007). This is even more evident in the Italian alpine region, due to its complex physiography coupled with local atmospheric patterns (Avanzi et al. 2015). Mean annual precipitation ranges from 500 (in the Aosta plain and inner Alpine valleys) to 3000 mm in some prealpine regions (Crespi et al. 2017). Based on areal values maximum (minimum) annual temperature is respectively 5 °C (−3 °C) in the Western and 8 °C (−1 °C) in the Eastern Italian Alpine sector (Esposito et al. 2014).

3 Data

3.1 Catalog of slope instability events

The catalog created for this work consists of 401 events of slope instability, which occurred between year 2000 and 2016 on the Italian Alps, at an altitude of more than 1500 m a.s.l. (Fig. 1). We considered all types of landslides, debris/

mudflows, glacial lake outburst floods, and ice avalanches. The choice of the starting date is related to the greater availability of climate records from weather stations in the last two decades. To build the catalog, we collected data from multiple sources. First, we relied on databases and technical reports realized by the Italian regional agencies: many data are freely available on the related geoportals (ARPA Piemonte 2018a; RAVdA 2018), and other data have been provided upon request. The dataset was then implemented with the information derived from the archives of CNR-IRPI Torino, from scientific papers and local/national newspapers (Luino and Turconi 2017; Paranunzio et al. 2016; Paranunzio et al. 2017). Additional information was obtained from firefighters' reports and online news of Civil Protection of Regione Autonoma di Trento (Protezione Civile - Provincia Autonoma di Trento 2018). More in detail, 53% of the inventoried case studies comes from Italian regional agencies and was partly collected in the framework of the Italian Landslide Inventory project (IFFI; Trigila et al. 2010), especially for the Veneto and Trentino regions; 27% of the case studies comes from the archives of CNR-IRPI Torino, while technical documentation and scientific works represent the 13% of the data sources. The source of information for each case study is shown in Online Resource 1.

Two main geographical clusters were identified, corresponding to the Western and Central-Eastern Italian Alps, respectively (Fig. 1). When considering the distribution and density of case studies in our catalog, one should bear in mind that they strongly depend on the availability of information. This latter, in turn, is mainly linked to the damage/risk associated with slope instability, rather than to its actual space/time distribution. This is particularly true for high-mountain areas, often remote and little frequented, where the information relating to slope instability events is often incomplete and fragmented. In these areas, summer events are more documented than events occurring in other seasons, due to the higher frequentation of high-mountain areas in that season. Likewise, information on natural instability events occurring at lower elevations is typically more readily available and more accurate and detailed, because these events more frequently interact with human activities and structures.

Online Resource 1 includes the information on the case studies that is relevant for this work (e.g., type of process, date, elevation and season of occurrence, volume and slope aspect). The case studies have been mapped as single points using a Geographical Information System (GIS) and Google EarthTM (Fig. 1). As mentioned before, data come from different sources: this could entail a certain degree of inhomogeneity for accuracy and level of detail. This is particularly true for newspapers that, in some cases, report general information and are only seldom precise enough about the location and time of triggering. Whenever available, the exact type of process has been reported: in the absence of precise information,

the slope instability process was generically classified as a "landslide." The accuracy of the spatial localization of case studies varies also according to the type of process. The starting point of landslides (of any type) is usually identified with a good accuracy. This information, instead, is rarely available for debris/mudflows, for which very often only the point of impact on structures and infrastructures is reported: if this point is below 1500 m a.s.l., and no information was available about the starting point, the event was not included in our catalog. As a result, debris/mudflows are underrepresented in our catalog. The percentage of the different types of slope instabilities contained in our catalog is shown in Fig. 1.

A digital elevation model with a 20-m resolution (SINAnet Ispra 2017) was used for the analysis of the topographical setting of the case studies.

3.2 Climate data

In order to reconstruct the climate history of each event of slope instability, we considered climate data from 131 automatic weather stations in Northern Italy (Fig. 1). These stations are managed by the Regional Environmental Protection Agencies (ARPA) in Piemonte (ARPA Piemonte 2018b), Lombardia (ARPA Lombardia 2018), and Veneto (ARPAV 2018) regions, by the Centro Funzionale of the Regione Autonoma Valle d'Aosta (Centro Funzionale Valle d'Aosta 2018), the Hydrographic Office of the Provincia Autonoma di Bolzano (Provincia Autonoma di Bolzano - Alto Adige 2018), and Meteotrentino (Meteotrentino 2018) in the Provincia Autonoma di Trento. We consider the following: (i) mean, maximum, and minimum daily air temperature (denoted as T_{mean} , T_{max} , and T_{min} , respectively, or simply T , from now on) and (ii) daily cumulated precipitations (rainfall and solid precipitation, denoted as R from now on). Temperature and precipitation values used in this work have been first validated by the regional agencies owning the data. Nevertheless, a further quality check has been done by the authors, in order to find out residual erroneous or anomalous values. Finally, temperature and precipitation data from 130 and 123 weather stations, respectively, were used. Information on the geolocalization, instruments, and source of the data is given in the Online Resource 1.

3.3 Data preparation

We establish a set of criteria to decide if the slope instability event could be included in the final sample, as follows. As anticipated in Section 3.1, we consider events (i) initiated above 1500 m a.s.l. and (ii) properly localized in space; beyond that, in order to enable a proper climate analysis, (iii) the date of occurrence has to be known with a daily accuracy. Details on the time/moment of the day are rarely available (only 12% of case studies).

We attribute a code to each case study, ranging from 1 to 3, describing the level of accuracy of the spatial localization: code 1 refers to events mapped with high accuracy (the detachment point is known); code 2 is mainly attributed to debris/mudflows, for which the exact detachment point is hard to know, but we know the channel where the flow developed; code 3 refers to the lower level of spatial accuracy (information on the elevation and failure zone are available, but not on the exact detachment point).

In order to identify the most suitable weather stations in the study area, we base the selection on three criteria, aimed to achieve the best compromise between the spatial distance from the failure zone, the representativeness of the morphological setting and the availability of climate data. More in detail, weather stations have (i) to be as close as possible to the failure zone, both in terms of altitude and horizontal distance; (ii) to be located in a morphological context similar to that of the failure area; and (iii) to provide a suitable temporal coverage (including the day of the event).

Whenever possible, weather stations located in the same valley where the slope failure occurred and in similar topoclimatic conditions are preferred (Nigrelli et al. 2018). As a second choice, we choose those stations that are located at a similar altitude and as close as possible to the failure area, at a horizontal distance lower than 20 km; otherwise, we select the available stations at lower elevations. The choice of a 20-km buffer zone is due to the need to rely on data that are representative of the climate conditions of the failure area: this is particularly crucial in complex-orography environments, as the Alpine region (Beniston et al. 2017). Stations with less than 10 years of climate records or with non-continuous data series are discarded. In case of weather stations measuring only one variable (T or R), we base the analysis of the event on two different, but nearby weather stations.

Given these strict requirements, in the end 358 events out of the original sample (401) are included in the final subset subject to climate analysis.

4 Methodology

The first steps of the method are addressed to the identification of climate variables assuming non-standard values at the date when a slope failure occurred (Sections 4.1 and 4.2). For these steps, we mainly rely on the methodology developed by Paranunzio et al. (2015) and modified by Paranunzio et al. (2016). In this way, we end up handling a multidimensional system, which may provide redundant information coming from variables showing similar patterns, making it complicate to find out the effective role of the climate forcing in the initiation of slope failures. We thus make a step forward, by performing a dimensionality reduction of the variables involved, as detailed in Section 4.3. This step is crucial, in order

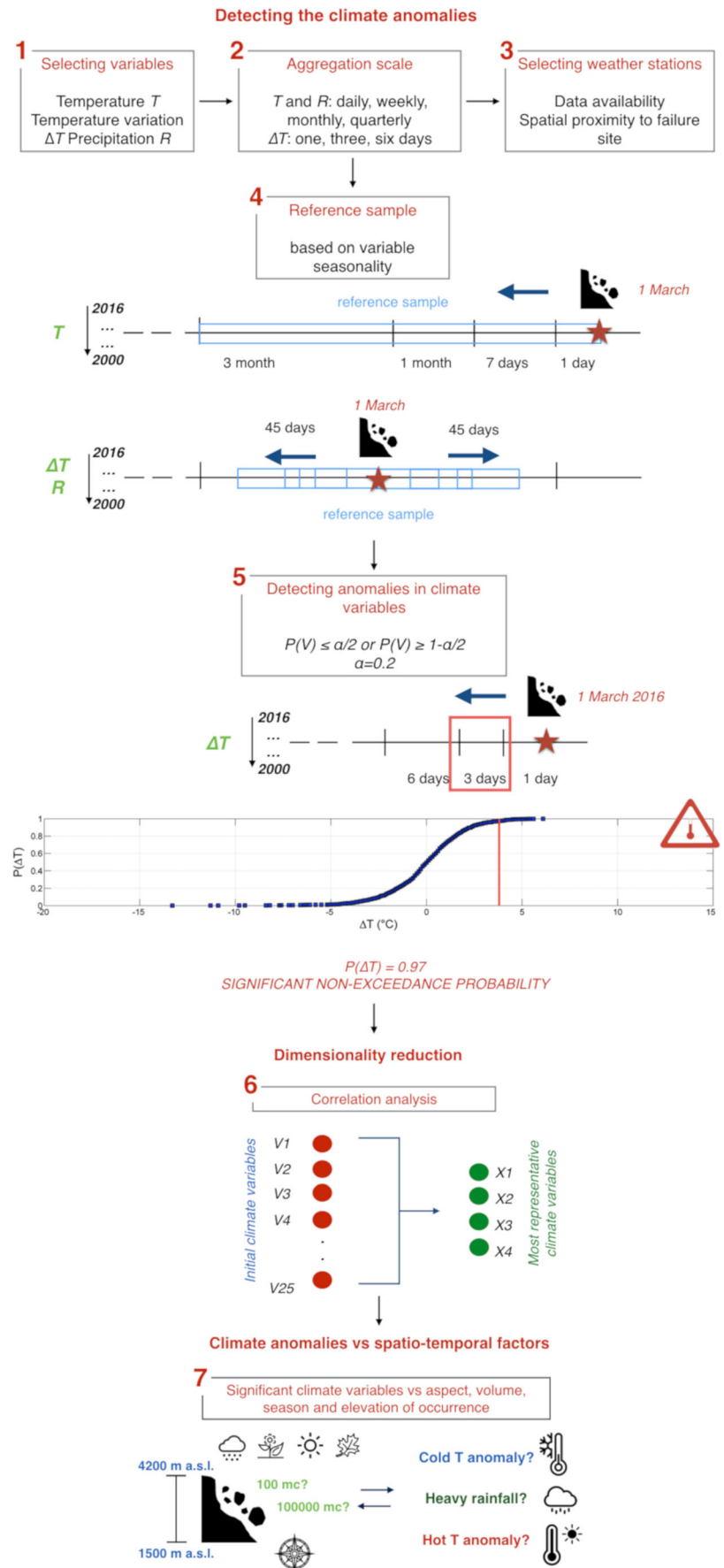
to identify the climate variables that are mostly involved in slope-failure initiation. We complete our study with some additional analyses taking into account the spatiotemporal distribution of the slope failures (Section 4.4), based on the set of climate variables selected in Section 4.3. The main steps of the procedure are illustrated in the flowchart of Fig. 2.

4.1 Detecting the climate anomalies potentially inducing slope-failure occurrence

The method adopted is a statistical-based approach, aimed to define the climate conditions in the period before a slope failure (the period from 1 day up to 3-months before the event), compared to the typical climatic conditions for the area of interest. In a first attempt, we perform the method with a bottom-up approach, i.e., without considering any a priori information on the event. Thus, by means of a non-parametric analysis based on the use of the empirical distribution function, we scrutinize the available sample data for each climate variable (V) in order to detect possible non-standard values in correspondence to slope-failure occurrence. The essential steps are reported below. Further details are available in Paranunzio et al. (2015, 2016). Hereinafter, we refer to the date of failure as “date” (e.g., 1 March 2016), whereas the calendar date is referred as “day” (e.g., 1 March).

- i. Selecting the climate variables: We use any easily available climate variable that could act as a trigger/preparatory factor of slope failure in climate-sensitive environments as high-elevation sites. We include temperature T , precipitation R (rainfall and solid precipitation), and temperature variation ΔT (i.e., the difference between the temperature at the day of occurrence of the slope failure and the value recorded in the day before or in an antecedent day).
- ii. Choosing the aggregation scale: V is the time-aggregated variable. For T and R , we consider time-aggregated variables from daily to quarterly scale. For ΔT , it is of interest to consider the temperature excursion between the day of failure and the previous days (1, 3, and 6 days in this work).
- iii. Selecting the weather stations: The choice of the most suitable weather stations for records collection is based on the requirements listed in Section 3.3.
- iv. Selecting the reference sample: We select the reference sample whereon comparing the variable V for the date of failure. The reference sample includes n values ($n \geq 10$) and $V_{(i)}$ is the i th value in the ordered sample, $i = 1 \dots n$. The choice of the reference sample depends on the seasonality of the variable involved. For T , we compare the value recorded at the date of the event with the values in the data series referring to the same period in other years. In the case of ΔT or intermittent processes as R , we extend the sample whereon performing the comparison to

Fig. 2 Flowchart representing the main steps of the method as in Section 4



include the previous and following 45 days, in order to increase the robustness of the analysis and to obtain larger reference samples.

- v. Non-exceedance probability value computation. We estimate the cumulative probability distribution $P(V)$ in a non-parametric way as $P(V) = i/n$, if $V > V_{(i)}$. We hypothesize that V may be a significant driver/trigger of a slope failure when $P(V) \leq \alpha/2$ (negative anomaly) or $P(V) \geq 1 - \alpha/2$ (positive anomaly). Here, we set the significance level set α at 0.2, performing a 10% test on each of the distribution tails. In the end, we consider V as a relevant factor for slope-failure occurrence when $P(V) \leq 0.1$ or $P(V) \geq 0.9$.

Note that we compute the probability distribution using data as they are recorded at the weather station, without transposing them at the detachment elevation, considering that a simple translation of values to the elevation of the slope failure would not modify the results. This assumption is discussed in detail in Paranunzio et al. (2015, 2016).

4.2 Towards the identification of a climate signal in the variables

After performing steps (i) to (v) as in Section 4.1 for all the considered variables, we obtain as many as 25 probability values per case study. These preliminary outcomes can be summarized in a $M \times L$ matrix, where M is the number of case studies included in the final sample and L is the number of climate variables (25 in this case). Each cell of the matrix reports the non-exceedance probability $P(V)$ associated with the j th variable, $j = 1 \dots L$, of the k th event, $k = 1 \dots M$. We claim that when $P(V) \geq 0.9$ we are in the presence of a positive anomaly in V , but of course the obtained value could also be the result of a random variation in V , which brought the V value above 0.9 by chance. This will happen on average in 10% of the cases, which entails that the variable brings a significant information at the regional scale only if the detected positive anomalies for that variable are more than 31, considering the example of Fig. 3, where the total number of considered case studies is 312. Instead of concentrating one's attention on the 0.9 probability, one can perform a graphical verification of the regional scale significance of the variable V for explaining slope instability occurrence. Consider the ordered sample of $M P(V)$ values, where each value is associated to an event and $M = 312$. $P(V)_{(k)}$ is the k th value in the ordered sample, $k = 1 \dots M$ for the j th variable. We compute the Empirical Cumulative Distribution Function (ECDF) as $q_{(j)} = k/M$, and we plot the q values versus their corresponding $P(V)$ value. We obtain a graph with 312 points, one for each event. If the points are close to the bisector, the variable is not significant at the regional scale in explaining slope instability

occurrence, because the points are positioned in the graph as if they were sampled randomly.

Conversely, curves that deviate significantly from the bisector are an indication of a variable being significant at the regional scale. If the points are positioned below the bisector line, in a considerable number of case studies the statistical analysis of the variable detects a positive anomaly. Similarly, curves above the bisector line refer to a more frequent presence of lower tail values (negative anomaly). As in the example of Fig. 3, we incur in a 19.5% of probability of detecting values above the 90th percentile, whereas just 5.4% of values is located in the lower tail of the distribution (10th percentile). The former value is almost twice the expected 10% significance, indicating the presence of an evident statistical positive climate anomaly at the daily scale.

The same approach is applied to all the considered variables. Ideally, we may detect as many as 42 positive and negative temperature anomalies, from the daily to the quarterly scale, for T_{mean} , T_{max} , and T_{min} , and four positive anomalies, from the daily to the quarterly scale, in precipitation values R . In this framework, a dimensionality reduction is of help in promoting the most important variables, by improving the interpretability of the final outcomes.

4.3 Reducing the dimensionality

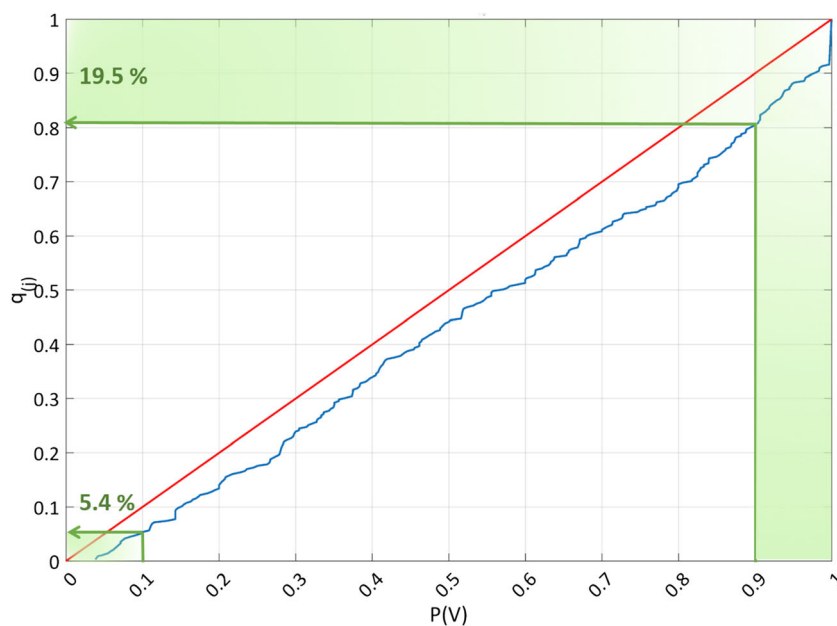
A dimensionality reduction is a procedure that allows one to reduce the initial number of considered variables (L) by obtaining a set of most important variables (S). We first perform a procedure based on correlation thresholds in order to detect variables that are highly correlated with others. The main steps are illustrated hereinafter. In the following points, we present some examples to make the methodology more clear.

- i. Computing the pairwise correlation coefficient: We calculate the Pearson correlation coefficient ρ , a dimensionless index measuring the linear correlation between couples of variables in columns i and j , as:

$$\rho_{ij} = \frac{\sigma_{ij}}{\sigma_i \sigma_j} \tag{1}$$

where σ_{ij} is the covariance and $\sigma_i \sigma_j$ is the product of the standard deviations. The coefficient ρ ranges between -1 and 1 , with 1 indicating perfect correlation, and -1 perfect anticorrelation. Based on the number of investigated variables (25 in this case), the output table is a 25×25 correlation matrix, i.e., the matrix with the correlation coefficients for all pairs of data columns.

Fig. 3 Empirical Cumulative Distribution Function (ECDF), denoted as $q(j)$, based on the probability values $P(V)$ of a j th variable for the entire sample (312 events in this case), as detailed in Section 4.2. The straight line indicates the bisector, whereas the curve indicates the ECDF. 19.5% of values lies above the 90th percentile, whereas only 5.4% of values are in the lower-tail (10th percentile)



- ii. Detecting highly correlated variables: We define a minimum correlation threshold $|\rho| = 0.5$, as suitable to identify pairs of variables with a high correlation. If the absolute value of the correlation coefficient is larger than 0.5, we mark the couple of variables as potentially redundant, because they bring a similar information into the system.
- iii. The pruning process starts from the couple of variables with the highest correlation; the variable is eliminated which contributes less to explain slope instability occurrence. As an example, $Tmax_1$ and $Tmean_1$ show a high correlation ($\rho = 0.87$); we eliminate $Tmax_1$, since $Tmean_1$ recognizes 24.9% of potential climatic anomalies, compared to 18% for $Tmax_1$. In cases when the potential anomalies recognized by the two variables are similar, we eliminate the variable with lowest number of available data. As an example, although $Tmin_{30}$ provides almost the same number of positive anomalies compared to $Tmean_{30}$ (17.5% and 17% respectively), we prefer the latter because $Tmean$ is measured at 312 weather stations, versus 275 for $Tmin$. We proceed with the pruning until all variables in the final subset have a correlation coefficient lower than 0.5 (in absolute value). We finally come out with a pool of the most significant variables, achieving a lower dimensional representation of a dataset, capable of preserving as much as possible the initial information.

4.4 Climate anomalies versus spatiotemporal factors

Finally, we perform a multivariate analysis in order to highlight complementary factors that, in combination with climate

anomalies, could help in the interpretation of processes leading to slope failure.

For this study, we considered the following: (i) season of occurrence, (ii) scar elevation, (iii) slope aspect, and (iv) detached volume. Events are divided in four seasonal classes based on the meteorological seasons. Four homogenous classes of elevation have been defined, ranging from the minimum to the maximum height of occurrence of the case studies. Aspect is expressed in degrees ($0\text{--}359^\circ$) and divided in four classes: north ($315^\circ\text{--}45^\circ$), east ($45^\circ\text{--}135^\circ$), south ($135^\circ\text{--}225^\circ$), and west ($225^\circ\text{--}315^\circ$) facing slopes. Case studies are finally grouped in two classes of volume, i.e., small events ($< 10^3 \text{ m}^3$), and large events ($\geq 10^3 \text{ m}^3$).

5 Results

5.1 Statistical analysis of the climate variables

The results of the analyses as in Section 4.1 are fully reported in the Online Resource 1 as a $M \times L$ matrix, where M is the number of case studies (358 in this case) included in the final sample and L is the number of climate variables (25 in this case). Thus, each cell of the matrix includes the non-exceedance probability $P(V)$ associated with the j th variable, $j = 1 \dots L$, of the k th event, $k = 1 \dots M$. Positive anomalies are in red, whereas negative ones are in blue. Positive anomalies refer to the upper-tail of the distribution ($P(V) \geq 0.9$), whereas negative ones refer to the lower tail ($P(V) \leq 0.1$). Information on the selected weather stations used for the analyses are also reported.

Figure 4 synthesizes the outcomes. Figure 4a displays the number of stations showing a positive/negative anomaly in the

considered variables, in association with slope-failure occurrences. There, we report the results of the data analysis of one station for each investigated event, being the total sample size equal to 358. Note that most stations provide T_{mean} and precipitation R data (312 out of 358 case studies), whereas T_{min} and T_{max} data are available for fewer stations (275 out of 358 case studies). We considered only the upper-tail of the distribution for precipitation, since low precipitation values are not a trigger of slope instability. Bold numbers immediately above the stacked bars indicate the number of stations for which the variable was available and has been analyzed, whereas upper/lower regular font numbers indicate the number of negative/positive anomalies detected for the considered variable. As an example, the variable T_{mean}_1 is recorded by 312 weather stations; thus, this variable was analyzed for 312 case studies (one event = one weather station), and a positive/negative anomaly was detected for 66 and 19 weather stations, respectively. In total, almost 27% of case studies show a statistical anomaly in T_{mean}_1 .

In general, as one can see from Fig. 4a, almost 30% of the weather stations used for this analysis show a positive/negative anomaly in most of the variables. Positive temperature anomalies mainly refer to T , in particular to T_{mean} , T_{max} , and T_{min} , at daily and weekly scales. Ranging from T_{mean}_1 to T_{min}_{90} in Fig. 4a, at least 18% of the analyzed weather stations provide a positive temperature anomaly (from 18.5% for T_{mean}_{30} to 26.2% for T_{min}_7). Negative anomalies are mainly referred to ΔT data: some variables present about 13% of stations with a negative temperature-variation anomaly (ΔT_{mean}_1 , ΔT_{min}_1 , and ΔT_{max}_3). More in detail, negative anomalies for these variables refer to a significant drop of temperature between the day of the failure and the previous one, 3 or 6 days. More than 20% of the analyzed stations show at least one precipitation anomaly (from 21% for R_1 to 29.4% for R_7).

Figure 4b reports the number of climate anomalies, associated with the occurrence of slope instabilities, for the considered case studies. In total, at least one anomaly is detected in 329 out of 358 events (91.9%). 47% of the analyzed weather stations shows from one to four anomalies in the long-term series, and 34.5% from five to nine anomalies. Only 8.1% of the events (29) does not show any anomaly in the climate variables, in association to slope instability occurrence. Based on the results shown in Online Resource 1, in 47% of the case studies (168), we detect one or more temperature anomalies, in just 7% (25 case studies) only a precipitation anomaly, and in almost 38% a combination of the two (136 case studies).

5.2 Identifying the key variables

As detailed in Section 4.2, we aim to find out the evidence of a climate signature in the occurrence of a slope

instability event. To this aim, we plot the empirical distribution functions of the values obtained by each variable in all case studies, for each of the 25 investigated variables, to have a visual validation of the significance of the considered variable in explaining slope instability at a regional scale.

Figure 5 shows the results for the entire sample of 25 variables. The percentages of values allocated in the upper/lower tails of the sampling distributions are indicated in the graphs (upper right and lower left sectors, respectively). As can be seen, focusing on the 90th percentile, the most significant variables are T_{mean} , T_{max} , and T_{min} and R , at all temporal scales (day, week, month, 3-months), together with ΔT_{min} (6 days). Confirming the results of Fig. 4, a major presence of negative anomalies is detected for ΔT . In this last case, the non-exceedance probability exceeds the expected significance in ΔT_{mean} (1, 3 days), ΔT_{max} (1 day), and ΔT_{min} (3, 6 days). Percentages above 10% are not of interest, since they are below the significance level.

A large number of variables is found to be statistically significant and, thus, potentially worth to be included in further analysis. On the one hand, this confirms the presence of evident climate signals associated with the occurrence of a slope failure in more than one variable; on the other hand, this entails a redundancy of information. For this reason, we tried to synthesize the information coming from variables showing similar patterns by performing the dimensionality reduction described in Section 4.3.

First, we quantify the correlation existing among all considered climate variables, by running a pairwise Pearson correlation analysis as described in Section 4.3. Darker colors indicate an increasing positive and negative correlation between the probability values associated to each pair of variables. Coefficients above the threshold $|\rho| = 0.5$ (indicating strong correlation) are in bold. As can be seen, T_{mean} correlates strongly at all temporal scales with T_{max} and T_{min} . A strong positive correlation across different temporal scales is detected in T_{mean} (daily/weekly and weekly/monthly scales), as well as in T_{min} . Strong correlations at different scales and between different variables are also detected (as for example $T_{mean}_{30}/T_{max}_{90}$ and $T_{mean}_{30}/T_{min}_{90}$). Similarly to T_{mean} , ΔT_{mean} correlates strongly with ΔT_{max} and ΔT_{min} at the same temporal scale (1, 3, and 6 days), and across different temporal scales (e.g., $\Delta T_{mean}_3/\Delta T_{mean}_6$, $\Delta T_{min}_1/\Delta T_{min}_3$, and $\Delta T_{min}_3/\Delta T_{min}_6$). Also, precipitation values strongly correlate at the daily/weekly and monthly/quarterly scales. As can be seen in Figs. 5 and 6, ΔT shows values that are often below the expected significance: for this reason, ΔT is discarded from the following analyses.

Starting from the couple of variables with the highest correlation (Fig. 6), we perform the pruning process as in Section 4.3. We first eliminate those variables contributing less to the explanation of slope-failure occurrence.

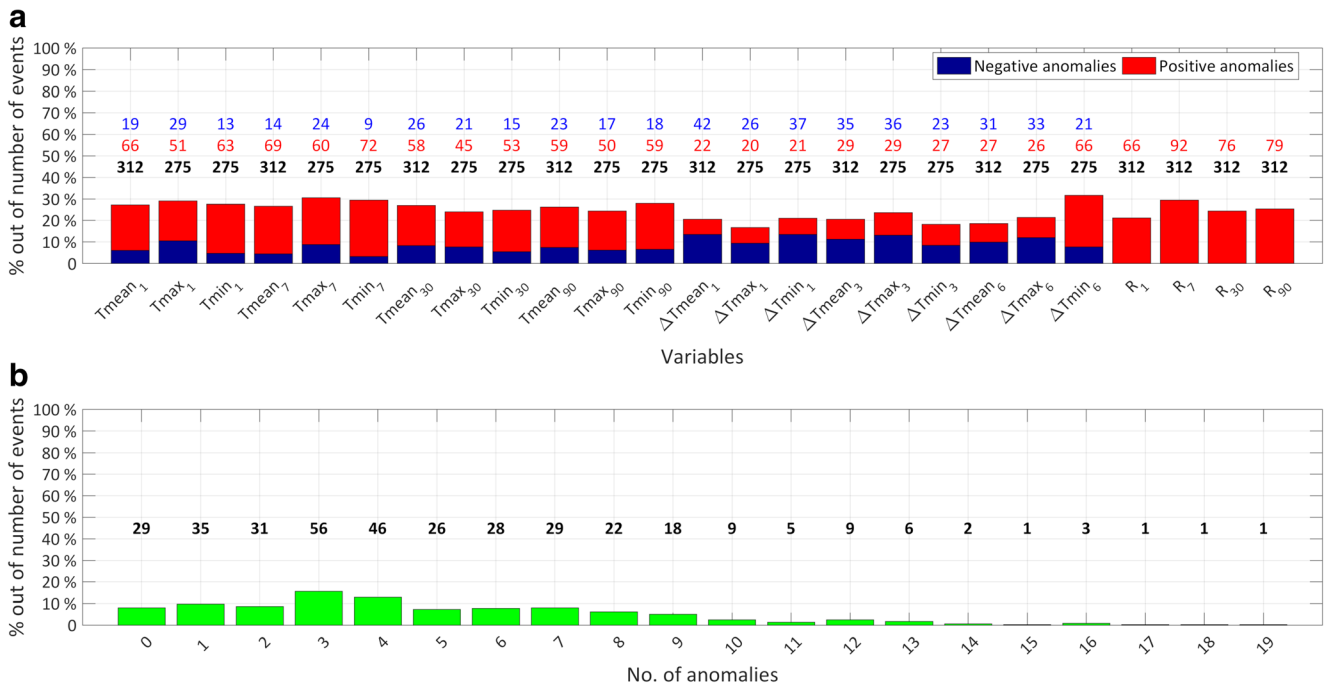


Fig. 4 **a** Number of climate anomalies per variable and percentage out of the total number of events (358). Lighter colors refer to positive anomalies (high extremes, heavy precipitation), darker color to negative anomalies (low temperatures). Numbers above the stacked bar, from the bottom to the top: number of available weather stations per variable, number of positive anomalies per variable, number of negative anomalies per variable. **b** Number of events (in bold) showing from 0 (no anomaly) to 19 climate anomalies and percentage out of the total number of events (358)

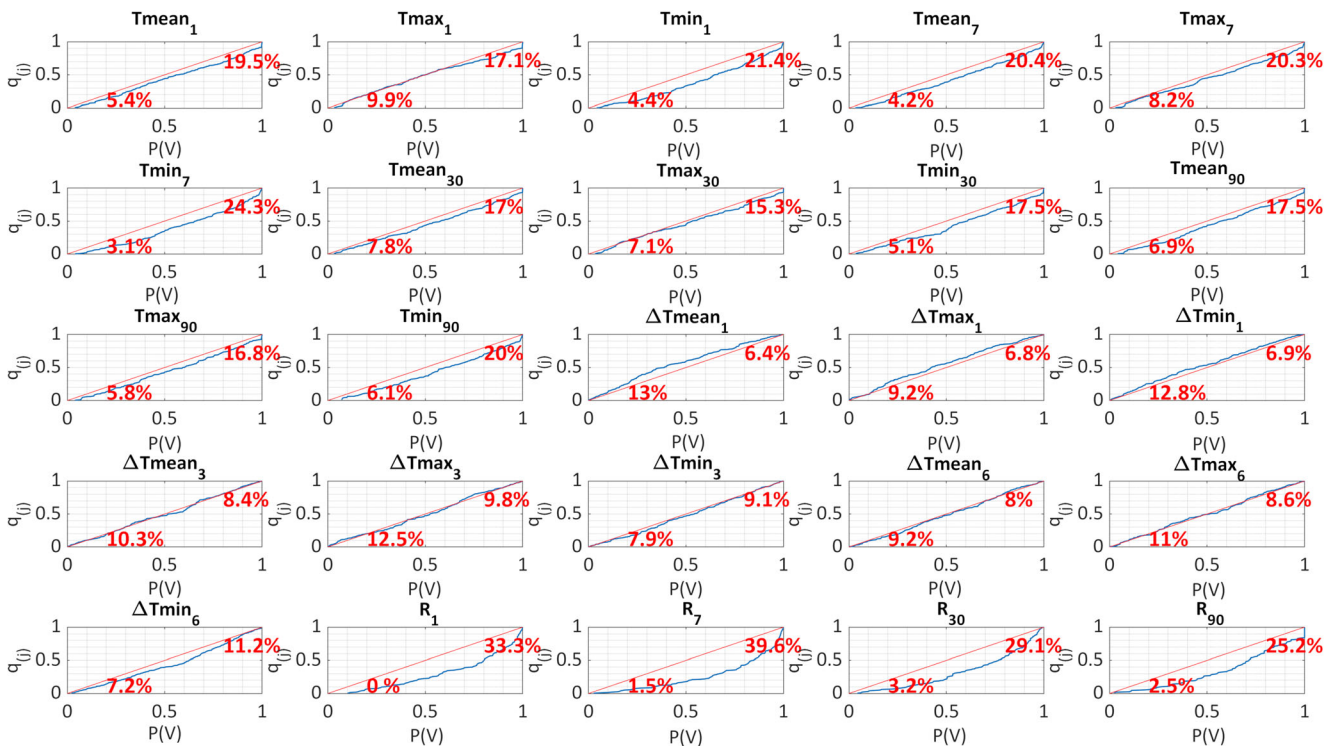


Fig. 5 Empirical Cumulative Distribution Function (ECDF), $q(j)$, based on the probability values $P(V)$ of the j th variable ($j=1 \dots L, L=25$) as detailed in Section 4.2. The straight lines indicate the bisectors, whereas the curves indicate the ECDF. Numbers in the lower left and upper right sectors refer to percentages of data below the 10th and above the 90th percentile, respectively

| P | Variables | | | | | | | | | | | | | | | | | | | | | | | | |
|----------------------------|---------------------------|--------------------------|--------------------------|---------------------------|--------------------------|--------------------------|----------------------------|---------------------------|---------------------------|----------------------------|---------------------------|---------------------------|---------------------|--------------------|--------------------|---------------------|--------------------|--------------------|---------------------|--------------------|--------------------|-----------------------|-----------------------|------------------------|------------------------|
| | <i>Tmean</i> ₁ | <i>Tmax</i> ₁ | <i>Tmin</i> ₁ | <i>Tmean</i> ₇ | <i>Tmax</i> ₇ | <i>Tmin</i> ₇ | <i>Tmean</i> ₃₀ | <i>Tmax</i> ₃₀ | <i>Tmin</i> ₃₀ | <i>Tmean</i> ₉₀ | <i>Tmax</i> ₉₀ | <i>Tmin</i> ₉₀ | $\Delta Tmean_{-1}$ | $\Delta Tmax_{-1}$ | $\Delta Tmin_{-1}$ | $\Delta Tmean_{-3}$ | $\Delta Tmax_{-3}$ | $\Delta Tmin_{-3}$ | $\Delta Tmean_{-6}$ | $\Delta Tmax_{-6}$ | $\Delta Tmin_{-6}$ | <i>R</i> ₁ | <i>R</i> ₇ | <i>R</i> ₃₀ | <i>R</i> ₉₀ |
| <i>Tmean</i> ₁ | 1.00 | 0.87 | 0.76 | 0.58 | 0.57 | 0.46 | 0.28 | 0.33 | 0.23 | 0.26 | 0.23 | 0.21 | 0.36 | 0.31 | 0.33 | 0.53 | 0.44 | 0.42 | 0.53 | 0.49 | 0.36 | -0.33 | -0.35 | -0.28 | -0.21 |
| <i>Tmax</i> ₁ | | 1.00 | 0.57 | 0.51 | 0.61 | 0.36 | 0.27 | 0.36 | 0.20 | 0.29 | 0.27 | 0.18 | 0.39 | 0.44 | 0.30 | 0.41 | 0.48 | 0.31 | 0.47 | 0.62 | 0.25 | -0.50 | -0.47 | -0.41 | -0.33 |
| <i>Tmin</i> ₁ | | | 1.00 | 0.49 | 0.42 | 0.51 | 0.27 | 0.28 | 0.29 | 0.21 | 0.14 | 0.20 | 0.14 | 0.04 | 0.31 | 0.43 | 0.30 | 0.52 | 0.43 | 0.32 | 0.57 | -0.11 | -0.19 | -0.19 | -0.14 |
| <i>Tmean</i> ₇ | | | | 1.00 | 0.92 | 0.87 | 0.54 | 0.56 | 0.49 | 0.33 | 0.32 | 0.26 | -0.05 | -0.01 | -0.10 | -0.16 | -0.16 | -0.16 | -0.04 | 0.01 | -0.10 | -0.11 | -0.26 | -0.29 | -0.22 |
| <i>Tmax</i> ₇ | | | | | 1.00 | 0.72 | 0.50 | 0.58 | 0.42 | 0.36 | 0.35 | 0.26 | 0.00 | 0.03 | -0.06 | -0.15 | -0.14 | -0.12 | -0.04 | 0.09 | -0.10 | -0.27 | -0.43 | -0.45 | -0.36 |
| <i>Tmin</i> ₇ | | | | | | 1.00 | 0.50 | 0.47 | 0.53 | 0.28 | 0.24 | 0.26 | -0.11 | -0.09 | -0.18 | -0.18 | -0.14 | -0.21 | -0.13 | -0.07 | -0.11 | 0.01 | -0.13 | -0.21 | -0.16 |
| <i>Tmean</i> ₃₀ | | | | | | | 1.00 | 0.90 | 0.92 | 0.59 | 0.52 | 0.52 | 0.01 | 0.03 | -0.04 | -0.06 | -0.01 | -0.06 | -0.22 | -0.08 | -0.18 | 0.01 | -0.03 | -0.17 | -0.10 |
| <i>Tmax</i> ₃₀ | | | | | | | | 1.00 | 0.78 | 0.58 | 0.64 | 0.48 | 0.01 | 0.06 | -0.04 | -0.04 | 0.00 | -0.02 | -0.19 | -0.05 | -0.18 | -0.13 | -0.16 | -0.32 | -0.23 |
| <i>Tmin</i> ₃₀ | | | | | | | | | 1.00 | 0.57 | 0.44 | 0.57 | -0.05 | -0.02 | -0.10 | -0.08 | -0.02 | -0.10 | -0.19 | -0.08 | -0.13 | 0.04 | -0.02 | -0.11 | -0.07 |
| <i>Tmean</i> ₉₀ | | | | | | | | | | 1.00 | 0.83 | 0.88 | 0.08 | 0.11 | -0.04 | 0.02 | 0.00 | 0.02 | 0.00 | 0.06 | -0.04 | -0.08 | -0.09 | -0.11 | -0.13 |
| <i>Tmax</i> ₉₀ | | | | | | | | | | | 1.00 | 0.72 | 0.02 | 0.10 | -0.05 | 0.01 | 0.00 | 0.01 | -0.04 | 0.02 | -0.11 | -0.15 | -0.14 | -0.17 | -0.17 |
| <i>Tmin</i> ₉₀ | | | | | | | | | | | | 1.00 | 0.00 | 0.06 | -0.09 | 0.01 | -0.01 | -0.03 | 0.00 | 0.03 | -0.01 | -0.08 | -0.08 | -0.07 | -0.06 |
| $\Delta Tmean_{-1}$ | | | | | | | | | | | | | 1.00 | 0.80 | 0.68 | 0.48 | 0.47 | 0.31 | 0.34 | 0.43 | 0.18 | -0.34 | -0.17 | -0.12 | -0.10 |
| $\Delta Tmax_{-1}$ | | | | | | | | | | | | | | 1.00 | 0.40 | 0.32 | 0.46 | 0.14 | 0.32 | 0.47 | 0.09 | -0.29 | -0.16 | -0.12 | -0.08 |
| $\Delta Tmin_{-1}$ | | | | | | | | | | | | | | | 1.00 | 0.52 | 0.43 | 0.56 | 0.36 | 0.33 | 0.32 | -0.25 | -0.13 | -0.14 | -0.15 |
| $\Delta Tmean_{-3}$ | | | | | | | | | | | | | | | | 1.00 | 0.85 | 0.79 | 0.54 | 0.41 | 0.47 | -0.22 | -0.16 | -0.12 | -0.05 |
| $\Delta Tmax_{-3}$ | | | | | | | | | | | | | | | | | 1.00 | 0.55 | 0.42 | 0.45 | 0.31 | -0.26 | -0.12 | -0.13 | -0.06 |
| $\Delta Tmin_{-3}$ | | | | | | | | | | | | | | | | | | 1.00 | 0.48 | 0.34 | 0.55 | -0.16 | -0.13 | -0.14 | -0.13 |
| $\Delta Tmean_{-6}$ | | | | | | | | | | | | | | | | | | | 1.00 | 0.84 | 0.80 | -0.21 | -0.25 | -0.08 | -0.08 |
| $\Delta Tmax_{-6}$ | | | | | | | | | | | | | | | | | | | | 1.00 | 0.54 | -0.37 | -0.28 | -0.15 | -0.17 |
| $\Delta Tmin_{-6}$ | | | | | | | | | | | | | | | | | | | | | 1.00 | -0.06 | -0.12 | 0.04 | -0.01 |
| <i>R</i> ₁ | | | | | | | | | | | | | | | | | | | | | | 1.00 | 0.57 | 0.37 | 0.24 |
| <i>R</i> ₇ | | | | | | | | | | | | | | | | | | | | | | | 1.00 | 0.61 | 0.40 |
| <i>R</i> ₃₀ | | | | | | | | | | | | | | | | | | | | | | | | 1.00 | 0.61 |
| <i>R</i> ₉₀ | | | | | | | | | | | | | | | | | | | | | | | | | 1.00 |

Fig. 6 Pairwise Pearson correlation coefficients among the 25 climate variables used for this work. Darker colors indicate stronger positive (numbers in bold) and negative (numbers in bold italic) correlation, respectively, whereas lighter colors indicate weaker correlation

The pruning process proceed until all variables in the final subset have an absolute value of the correlation coefficient lower than 0.5. In case of similar potential anomalies recognized by the two variables, we select the variable with the highest availability of data. Considering the greater availability of weather stations recording *Tmean* compared to *Tmax* and *Tmin*, we select the former variable as being the most representative, along with *R*. For these variables, the non-exceedance probability is greater than the expected significance only in the upper-tail (Fig. 5); thus, we focus solely on positive anomalies. The choice of the variables to be selected is thus a matter of achieving a suitable number of representative variables and the need to minimize redundancy. In the end, we decrease the dimensionality of the problem to four variables, two for the short-term range and two for the longer one: (i) *Tmean*₁, (ii) *Tmean*₃₀, (iii) *R*₁, and (iv) *R*₃₀.

The final results related to the four selected variables are illustrated in the form of contingency table as in Table 1. Each cell represents the frequency distribution of one or more variables at a time. Values on the diagonal refer to the percentage of events whereon only the variable in the *i*th row (*i* = 1...4) resulted to be significant, whereas each off-diagonal element is the percentage of events whereon the variable in the *i*th row is significant in concomitance with another variable in the *j*th column (*j* = 1...4), *j* ≠ *i*. The last column indicates the percentage, out of the total sample size, for which the variable in the *i*th row is detected as statistically significant, alone, or in association with the other variables in the *j*th columns. In other words, this percentage indicates the percentage of case studies where the variable is a potential driver of slope instability.

In order to guarantee a statistical homogeneity of the sample, we now consider only the case studies for which both

Tmean and *R* data are available, i.e., 317 out of the total number of case studies (358). As an example in Table 1, *Tmean*₁ is significant in 10.7% of the analyzed 317 events, and 1.6% of events show a double anomaly in both *Tmean*₁ and *R*₁, while 18.5% of events in total are related to a significant anomaly in the *Tmean*₁. As can be seen from Table 1, results are well above the expected significance for all the variables. Precipitation at the long-term shows the most evident signal, which is associated with 21.3% of case studies, followed by a short-term high temperature (18.5%), heavy short-term precipitation (17.6%), and, finally, long-term positive temperature anomaly (15.7%).

5.3 Spatiotemporal distribution vs key variables' climate anomalies

Results of the statistical analysis are shown in the following Figs. 7 and 8. Based on the results of the dimensionality reduction performed in Section 5.2, we select two climate variables that are representative of short-term temperature and precipitation anomalies (*T*₁ and *R*₁) and two for the longer-term (*T*₃₀ and *R*₃₀). A slope-failure event could be related to

Table 1 Contingency table among the selected climate variables and related statistics out of 317 case studies

| Selected climate variables | Selected climate variables | | | | |
|----------------------------|----------------------------|----------------------------|-----------------------|------------------------|-------|
| | <i>Tmean</i> ₁ | <i>Tmean</i> ₃₀ | <i>R</i> ₁ | <i>R</i> ₃₀ | Total |
| <i>Tmean</i> ₁ | 10.7% | 4.4% | 1.6% | 1.9% | 18.5% |
| <i>Tmean</i> ₃₀ | 4.4% | 9.1% | 1.6% | 0.6% | 15.7% |
| <i>R</i> ₁ | 1.6% | 1.6% | 6.9% | 7.5% | 17.6% |
| <i>R</i> ₃₀ | 2.2% | 0.6% | 7.5% | 11.0% | 21.3% |

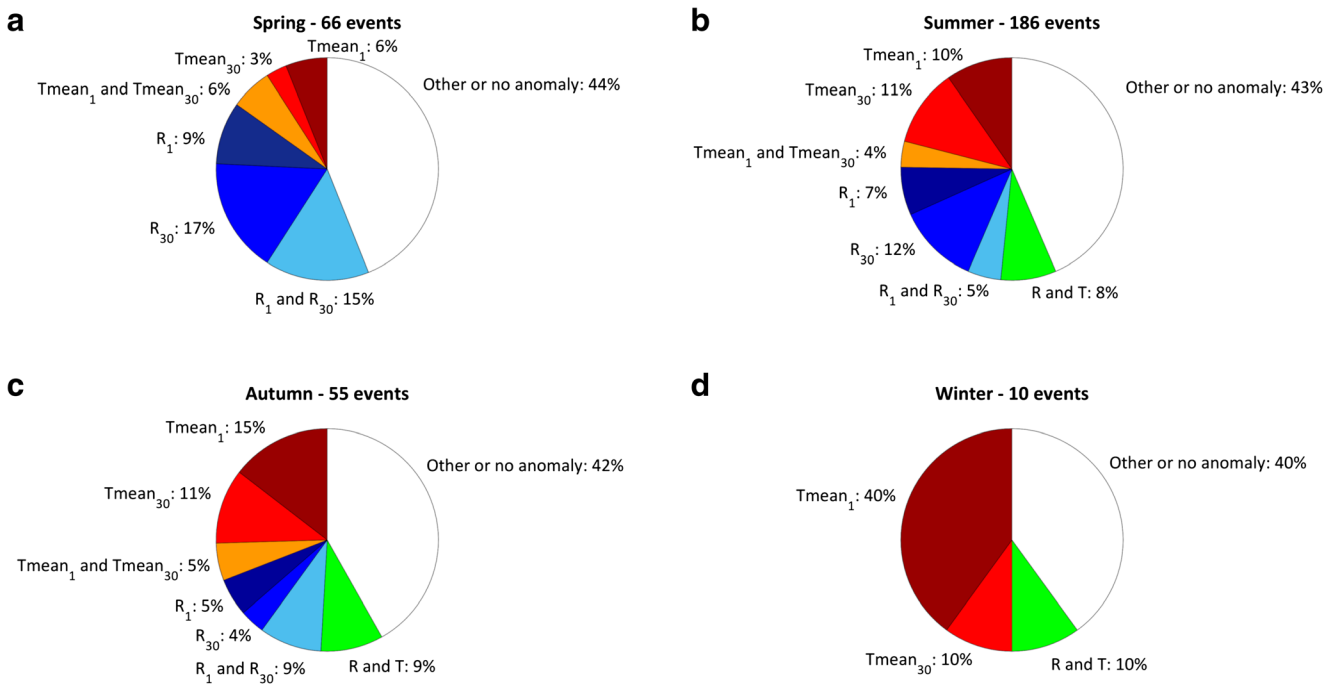


Fig. 7 Climate anomalies based on the selected climate variables across season of occurrence. Short-term temperature anomaly: $Tmean_1$, long-term temperature anomaly: $Tmean_{30}$, widespread temperature anomaly: $Tmean_1$ and $Tmean_{30}$, short-term precipitation anomaly: R_1 , long-term

precipitation anomaly: R_{30} , widespread precipitation anomaly: R_1 and R_{30} , both temperature and precipitation anomaly: R and T , no detected anomaly in the four selected variables: Other or no anomaly

more than one climate variable at a time. In other words, a combination of climate anomalies could be detected for a specific case study, e.g., T_1 and R_{30} or T_1 and T_{30} . Thus, to better

interpret the climatic framework leading to slope failure, a clusterization of the selected variables in eight groups is performed, as follows.

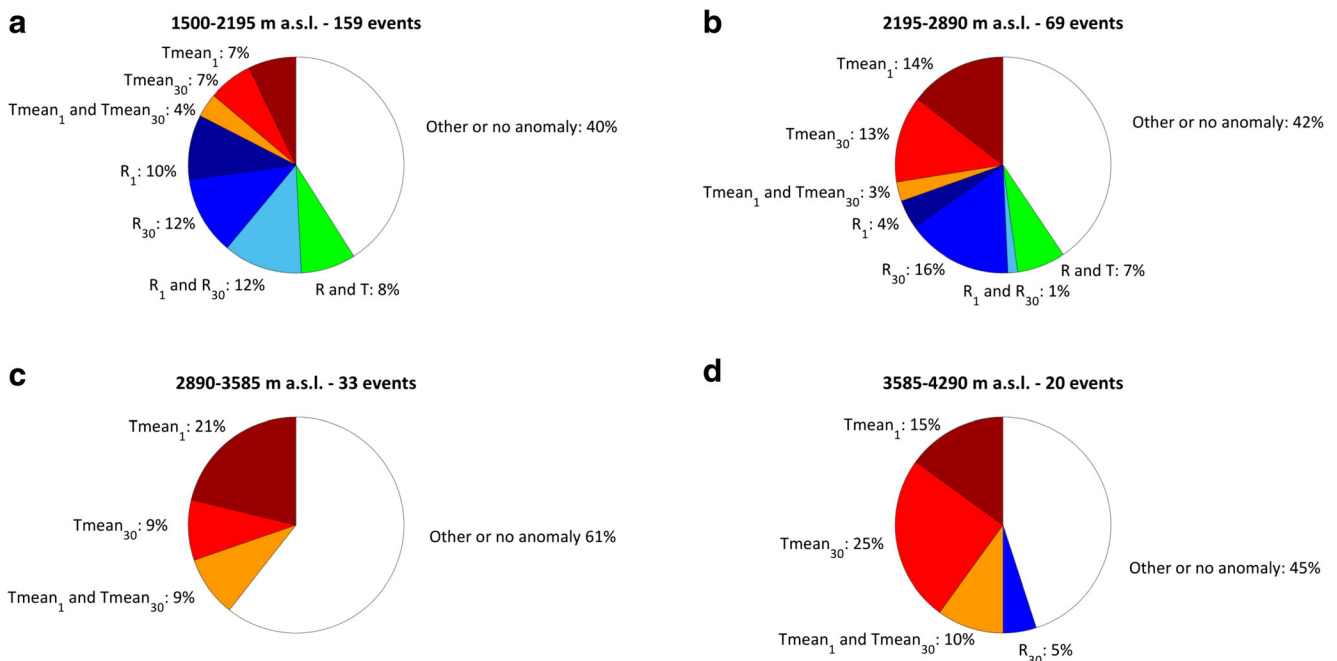


Fig. 8 Climate anomalies based on the selected climate variables across elevation of occurrence. Short-term temperature anomaly: $Tmean_1$, long-term temperature anomaly: $Tmean_{30}$, widespread temperature anomaly: $Tmean_1$ and $Tmean_{30}$, short-term precipitation anomaly: R_1 , long-term

precipitation anomaly: R_{30} , widespread precipitation anomaly: R_1 and R_{30} , both temperature and precipitation anomaly: R and T , no detected anomaly in the four selected variables: Other or no anomaly

- T_I (short-term positive temperature anomaly);
- T_{30} (long-term positive temperature anomaly);
- T_I and T_{30} (widespread positive temperature anomaly);
- R_I (short-term precipitation anomaly);
- R_{30} (long-term precipitation anomaly);
- R_I and R_{30} (widespread precipitation anomaly);
- T and R (both temperature and precipitation anomaly of any type);
- Other or no anomaly (no anomaly in the four selected variables).

Note that 180 events out of 317 are related to almost one anomaly in the four selected variables. The remaining 137 are linked to statistical anomalies in the other 21 discarded variables or unrelated to climate forcing (Other or no anomaly group). In this section, we present the main results, further analyses are included in the Online Resource 2 and briefly illustrated at the end of this paragraph.

Results shown in Fig. 7 highlight that summer events definitely prevail (58.7% out of 317 events), whereas winter events are the smallest group (3.2% out of 317 events). Proportions are almost the same if compared to the initial sample of 358 events, with 20%, 57.5%, 19%, and 2.8% of case studies occurring in spring, summer, autumn, and winter, respectively. Most of the events occurred in spring (Fig. 7a) are associated with an anomaly in precipitation values (41%), mainly in combination with prolonged precipitations (R_{30}), while T anomalies are detected only for 15% of the case studies. Summer events (Fig. 7b) are almost equally distributed between T (25%) and R (24%) anomalies. In autumn, temperature plays a major role, in combination or not with precipitation (Fig. 7c), and this is even more clear for winter events, even if in this latter season the sample of case studies is very limited (Fig. 7d). In general, positive temperature anomalies are relevant in spring and summer months. The case studies not associated with anomalies in the four variables selected are distributed homogeneously among seasons.

In Fig. 8, we analyze climate anomalies' distribution across four elevation ranges, obtained from a homogeneous subdivision based on the minimum and maximum height of occurrence of the case studies. It has to be pointed out that most debris/mudflows are located in the lowest elevation range, since, in general, the exact initiation point is hardly documented and only information on the deposition area, where damage usually occurs, is available. As can be seen, precipitation anomalies prevail at lower elevations, whereas the presence of positive temperature anomalies is more and more evident at higher elevations. Precipitation anomalies of different type (short/long term, widespread) are detected in the lowest range (Fig. 8a), whereas the long-term one is predominant in the mid-range (Fig. 8b). Case studies showing no anomaly in the four selected variables are mainly located in the mid-range (Fig. 3c).

With regard to the type of slope instability, we grouped the case studies in two main clusters, the first including rock/blockfalls, rock avalanches, landslides, icefall/avalanches, soli slips, and slides (from now on, "landslides") and the second including debris/mudflows and Glacial Lake Outburst Floods (from now on, "debris/mudflows"). Landslides are mainly associated to positive temperature anomalies (25%, if considering short/long term and widespread anomalies) and to long-term precipitation anomalies (12%), whereas short-term precipitation anomalies slightly prevail in association with the occurrence of debris/mudflows. Overall, in the case of debris/mudflows, a major combined contribute of precipitation and temperature is detected (12% of events) with respect to landslides (5%). Most part of case studies showing no anomaly in the four selected variables are landslides (48%). Graphs are available in the Online Resource 2.

Case studies have been grouped in four classes according to slope aspect at the initiation point (Online Resource 3): no strong indication was detected of a preferential distribution of the events among the different climate anomalies in relation to slope aspect, with the exception of a 35% of N-facing slope instabilities occurred in association with a temperature anomaly (mainly long term), in combination or not with precipitation. The case studies not associated to anomalies in the four variables selected are distributed homogeneously among slope aspects.

With regard to the magnitude of the events (Online Resource 4), we have data only for about 40% of the case studies, i.e., 128 events out of 317: for this reason, and for the uncertainty that is sometimes associated with volume assessment, only two classes of volume have been defined, i.e., small ($< 1000 \text{ m}^3$) and large ($\geq 1000 \text{ m}^3$) slope instability events. Small-volume events are more numerous and almost equally distributed among temperature and precipitation anomalies. Large-volume events are more often related to extreme temperatures (33% of events, by summing short, long, and widespread anomalies). As can be seen in Online Resource 4, almost half of the case studies in both classes of volume are not associated to anomalies in the selected variables.

6 Discussion

The main results of the study are hereinafter discussed by re-connecting to the main research questions raised in the introduction.

- (i) Can temperature and precipitation be considered as key conditioning and/or triggering factors for slope failures at high-elevation sites? Which climate variables are the most relevant for slope instability?

According to our analyses, almost 92% of the case studies is associated with one or more anomalies in the climate variables. Obviously, this does not necessarily imply a direct and univocal cause-effect relation between anomalous values of the climate variables and initiation of slope instability. However, this result is a clear evidence that climate variables (both T and P , at various timescales) are key factors for slope instability. At the same time, our analysis sheds light on the high heterogeneity of the type of anomaly/ies detected on occasion of the occurrence of a slope instability event, confirming what is known about the complexity of the diverse mechanisms leading to slope failure. In such a framework, the number of case studies collected in this dataset provides the ground for robust and significant conclusions about the nexus between climate variables and slope-failure occurrence. This result is an improvement with respect to Paranunzio et al. 2016, where the number of considered events was 41 compared to 401 in the present paper. Paranunzio et al. (2016) were able to associate a climate anomaly to 85% of the case studies, which is consistent with the result obtained here (92%), also in view of the fact that in the present paper we have enlarged the set of considered climatic variables.

Through the dimensionality reduction, we detect four key climate variables: T_{mean_1} , $T_{mean_{30}}$, R_1 , and R_{30} . Significant positive climate anomalies prevail as the drivers of slope instabilities, i.e., heavy precipitation and high temperatures. Precipitation at the long-term shows the most evident signal. Heavy, prolonged precipitations act in depth, altering soil moisture and slope hydrological conditions (Ma et al. 2014). Rainfall is a recognized trigger of landslides (e.g., Jakob and Lambert 2009), and the role of heavy prolonged rainfall has been widely discussed in the past (e.g., Luino 2005). In the recent years, the role of temperature as a potential trigger of slope instability has been investigated (e.g., Allen and Huggel 2013) and statistically verified by Paranunzio et al. (2016). The results of this work, based on a larger sample, confirm this evidence. Our results show that most of the events are associated with a temperature anomaly, in combination or not with precipitation non-standard values (47% and 38%, respectively). These results strongly support the hypothesis, already put forward by many authors (e.g., Geertsema et al. 2006), that global warming can be deemed responsible for an increase of slope instability, in particular in high-elevation/latitude areas, where the cryosphere plays a crucial role in conditioning slope dynamics.

The dimensionality reduction, on the one hand, entails a cost in terms of ability to associate a specific case study to a climate anomaly, but on the other hand, it has many advantages. First of all, this approach allows one to identify climate anomalies also when few climate variables are available. This is the case of most of the weather stations located in high-mountain areas: often these weather stations register only few variables (mostly T_{mean} , as evidenced in the previous

sections), and we can thus rely on a limited set of climate records. Moreover, this dimensionality reduction procedure facilitates the visualization, classification, and interpretation of the results.

(ii) How can the detected climate signal be linked to the process typology and to its spatiotemporal distribution?

As already mentioned, in our sample “landslides” (including all different types, 239 case studies) sharply prevail on “debris/mudflows” (78 case studies). This asymmetric distribution is mainly due to the fact that most information about debris/mudflows is related to the transition/accumulation area (where damage is produced), rather than to the starting zone. This means that, if the damage/accumulation/transition area was at an elevation lower than 1500 m, the event was discarded. Keeping this bias in mind, we notice that debris/mudflows are better explained by the four key climate variables than landslides, with a major role played by precipitations, at all temporal scales. This picture, on one side, confirms some already well-known facts. Debris/mudflow initiation is mainly driven by precipitation (e.g., Jakob et al. 2012), even if their occurrence is the result of a combination of not only water (mainly from rainfall, but occasionally from snow/ice melt or GLOF), but also debris availability (from landslides, scarp and/or channel bed erosion; at high-elevation, (post)glacial deposits may represent an important sediment source areas, Turconi et al. 2010). Landslides, instead, are the result of more complex processes, which depend on landslide type. On the other side, our results suggest that, at high elevations, temperature plays a crucial role not only in landslide initiation, as it has been widely recognized, but also in debris/mudflow initiation: temperature’s contribution to the initiation of this latter type of process is something that is less understood and debated (Stoffel et al. 2011). On this regard, it is interesting to notice that, among temperature anomalies, long-term ones prevail on short-term ones for debris/mudflows, while the opposite is true for landslides: according to this, we may speculate that high temperatures are mainly a preparatory factor for debris/mudflows (e.g., through snow/ground-ice melt which saturate the debris, Wieczorek and Glade 2005, Geertsema et al. 2014) and a triggering factor for landslides (e.g., by snowmelt, Cardinali et al. 2000).

Half of the case studies are concentrated in the lowest elevation range, and the number of case studies decreases rapidly with elevation. Low-elevation areas are in fact wider and more frequented, and the probability that slope instabilities are reported is therefore greater. Despite the relative lack of data at the highest elevations, an increasing role of positive temperature anomalies with elevation, on extended timescales clearly emerges: in particular, at the highest elevations (> 2890 m a.s.l.) precipitation is not a significant forcing for slope instability. This is a clear indication of the crucial role

played by cryosphere dynamics in the development of slope instability in high mountains (Deline et al. 2015). Long-term temperature anomalies may be responsible for permafrost degradation/thawing in depth (Gruber and Haeberli 2007); interestingly, this is the most significant climate variable at the highest elevations (> 3500 m a.s.l. approximately). Short-term temperature anomalies affect near-surface dynamics: in permafrost environments, temperature variations and short-term extremely warm conditions could affect rock stability within hours through rapid thawing processes (Hasler et al. 2012). It is also interesting to notice that only a small part (39%) of case studies in the elevation range 2890–3585 are associated with anomalies in the four key climate variables. An explanation for this may be in the fact that at this elevation range, in recent times, the most important changes in permafrost and glacier extent occurred: additional processes, developing at timescales larger (pluriannual) than those investigated here, may be responsible for slope instability occurrence, e.g., slope debuttressing as a consequence of glacier retreat (Geertsema and Chiarle 2013).

As for the seasonal distribution, summer events sharply prevail, whereas spring and autumns ones are almost balanced; winter events are the clear minority. The concentration of case studies in summer is partly due to some inhomogeneity in data reporting, considering that frequentation of high-mountain areas is the highest in this season. Besides this, we can observe that most of the spring events occur in the presence of some extraordinary precipitation (41%), whereas this type of anomaly decreases gradually in summer and autumn, to almost disappear in winter. In this last case, we have to consider that winter precipitation recorded by high-elevation weather stations is only partly reliable, because of undercatch bias when precipitation is in solid form (Buisan et al. 2016). It is interesting to notice how the relative importance of precipitation among seasons only in part reflects the pattern of climate variables during the year. In particular, precipitation is as important as temperature during summer, when we might expect a predominant role of temperature. On the opposite, temperature is more relevant than precipitation in autumn, a season generally associated to heavy precipitations. In this regard, it has been observed that permafrost active layer reaches maximum depths in late autumn, when the ground surface is already in freezing conditions (Magnin et al. 2016): this situation may lead to water pressure build-up in the slope, up to its failure. The association of winter events with short-term temperature anomalies is the most difficult to explain, even if the number of case studies for this season is so little, that any outcome has to be considered very carefully. For these cases, we may speculate that, on steep slopes, where only little snow can accumulate, short-term warm conditions may cause snowmelt, able to trigger the slope instability. Since winter events are in general large events, we should consider a water input from snowmelt only as the trigger of unstable conditions,

generated perhaps by water pressure build-up, as discussed for autumn events.

The distribution of case studies and of the related anomalies in relation to slope aspect does not reveal any relevant pattern. Temperature and precipitation anomalies at various temporal scales are quite homogeneously distributed on the different slope aspects. Only the north-facing slopes show a slightly higher sensitivity to temperature anomalies, in particular to long-term ones (15%). This is in agreement with the findings of some studies that identify north slopes as the most sensitive to temperature increase, because of the thinner permafrost active layer. For east-facing slopes, a relative importance of short-term temperature (15%) and long-term precipitation (16%) anomalies is highlighted: the significant association of events with short-term temperature anomalies may be related to the higher solar radiation received by these slopes. For these types of analyses, it would be important to consider among climate variables also solar radiation, for which however, at the moment only few data are available for the Italian Alps.

The analysis of anomalies' distribution in relation to the size of slope instability highlights how the four key climate variables are less able to catch a climate signal in association with large events, than with small events. This quite predictable outcome can be explained by the higher complexity of processes and mechanisms involved in the occurrence of large-scale slope instabilities (Crozier 2010). What is interesting, however, is that, quite surprisingly, very few large-volume case studies are associated with precipitation, while temperature, and in particular short-term anomalies (18%), appears to be a significant climatic driver. We may conclude that, for large-volume events, our approach is able to catch the climate anomaly eventually associated to the triggering of slope instability but cannot shed light on the complex set of processes involved in its setup. A different approach, considering more extended (annual/pluriannual) timescales and predisposing factors, such as the lithological and structural setting (Fischer et al. 2012), not directly related to climate, would be necessary, but this is out of the scope of this work.

- (iii) Can climate change be deemed responsible for the observed increasing trend of slope instability at high elevation?

The answer to this question is very complex. In order to respond unambiguously, we should have, as is the case of climate data, long-term datasets, allowing the identification of trends in the occurrence of slope instability. Unfortunately, even today, the reporting of these events strongly depends on the associated damage/risk, so that the available data series are incomplete and inhomogeneous and thus unsuitable to provide trends to be compared with climate variations. Even if some authors attempted to fill this gap using different approaches/

techniques, results are nevertheless partial and/or of local value. In addition, as already mentioned, slope instability is the result of a complex set of processes that respond with different velocity and amplitude to climate change.

In this complex framework, the results of this study, while not being able to unambiguously prove/disprove the role of climate change on slope instability increase at high elevation, strengthen this hypothesis. Three out of the four key variables detected can be attributed to pattern of climate change and global warming scenarios (i.e., T_I , T_{30} and R_I). The robust sample investigated in this work and the high number of case studies occurred in the presence of positive temperature anomaly support the hypothesis of a climate signal in the initiation of mass-wasting processes at high-elevation sites, as suggested by previous studies (e.g., Allen and Huggel 2013). Based on the results of this work, precipitation at the longer term scale (R_{30}) is the main climate forcing related to slope-failure occurrence. According to the scenarios of climate change, reduced total amount of precipitation in the Southern European Alps are expected (Brunetti et al. 2009; Gobiet et al. 2014), and thus, also a reduction of slope instabilities induced by prolonged abundant precipitation is hypothesized (e.g., Dehn et al. 2000). Conversely, the effect of intense short-term precipitation (as R_I) on the initiation of slope instability events could be more and more evident in the next future (Gariano and Guzzetti 2016).

As cryosphere degradation proceeds up to its complete disappearance, we might anticipate a decreasing impact of global warming on slope stability at high elevation/altitude. However, taking into account recent studies highlighting the role of diurnal thermal stressing in unstable rock masses also in non-cryospheric areas (Collins and Stock 2016), where warming-cooling cycles can gradually affect rock mechanics, leading to slope failure, we may conclude that T , and in particular global warming will continue to impact on slope instability also in a scenario of a vanishing cryosphere.

If the role of extraordinary warmth in destabilizing rock mass has been widely analyzed by recent works (e.g., Gruber and Haeberli 2007; Collins and Stock 2016), little attention is paid to negative anomalies as potential drivers of slope instability. Our analysis pointed out that a significant number of events were associated with negative values of ΔT , i.e., with sudden temperature drops in the day(s) preceding the failure. Build-up of water pressure (e.g., freezing of water springs) or rock damage due to freezing-thaw cycles are among the different mechanisms that, in association with temperature drops, can lead to slope failure, depending, among others, on the type of instability process, season of occurrence, and lithological and geomorphological features (Fischer et al. 2012). Climate change may influence also these processes, through an increase of temperature variability (Schar et al. 2004), and thus of the probability of sudden temperature drops/raises.

In the end, we recall some important points and constraints that have to be kept in mind, when analyzing the results of this work. First of all, we base our analysis on a relatively short period (from 2000 on): this is due to the need of disposing of sufficient information on temporal and spatial localization of the events and of reliable and consistent data from the weather stations.

We are aware that, in mountain regions, many factors affect the measure of the climate variables at a site, complicating the climatological framework whereon we operate, as the scarce coverage of long-term weather stations at high elevation in Italy. In these remote areas, automatic weather stations have been installed recently and, in general, only cover the last 15–20 years (Pepin et al. 2015). This entails relying sometimes on measuring stations far from the study area and, thus, not fully representative of the climate conditions of the detachment area. This is particularly evident for precipitation, which is affected by a larger spatial variation in high-mountain areas with respect to temperature (Isotta et al. 2014). To limit these problems, as illustrated in Section 3.3, we first fix a series of requirements when selecting weather stations, in terms of data availability, length of the historical data series, and distance from the failure area. Moreover, the method as is allows one to detect the climate anomaly directly at the station, thus overcoming the problem related to the elevation of the instrument.

The data heterogeneity, due to the fact that in Italy there are several meteorological data source, and the different length of the historical data series could introduce bias into the records (Merlone et al. 2015). However, this does not affect the estimation of the probability values, since we compare the value of the date of failure occurrence to climate data recorded at the same reference instrument and not among different weather stations. The availability of new products based on a merging and/or combination of gridded data and in situ climate records could be a way to partially overcome the shortcoming related to lack and inconsistency of climate data, but the relatively low spatiotemporal resolution of remotely sensed records with respect to our scale of analysis is another major limiting factor in this context (Mountain Research Initiative EDW Working Group 2015).

7 Conclusions

In this work, we collected an inventory of 401 slope instability events and finally analyze 358 case studies, documented from 2000 to 2016 in the Italian Alps, at elevations above 1500 m, with the aim to assess the role of climate forcing, and an eventual signal related to climate change. This dataset is something unique in the world for mountain regions, considered not only the number of case studies but also the quality of their spatiotemporal localization. First of all, we tested on this robust and diverse dataset the statistical approach proposed by

Paranunzio et al. (2015, 2016), which allows one to define in a standardized way the climate signal behind a slope-failure event. In order to make a step forward towards a quantitative attribution of the effect of global warming in the observed increasing mass-wasting activity at high elevation, in this work, we implemented a procedure for the identification of the essential climate variables associated with slope-failure occurrence. Although some critical points still remain, as outlined in the previous paragraph, some important conclusions can be drawn from this work, as listed hereinafter.

- (i) More than 90% of the 358 investigated events occur in the presence of one or more of the 25 climate anomalies considered. For this high-elevation dataset, temperature was confirmed as a fundamental climate variable: in 47% of cases, we detect a temperature anomaly, in 38% a combination of temperature and precipitation anomalies, and only in 7% of cases solely a precipitation anomaly.
- (ii) The dimensionality reduction from 25 to 4 key climate variables reduced the sample size to 317, but allowed us to decrease the noise created by redundant information and to catch the most evident climate signals behind slope instability.
- (iii) The key climate variables that resulted to have positive anomalies in association with 57% of the 317 case studies are T_{mean_1} and $T_{mean_{30}}$, R_1 and R_{30} . Precipitation at the long-term shows the most evident signal (21.3% of case studies associated to anomalous values of this variable), followed by short-term temperature anomalies (18.6%).
- (iv) Considering the four above-mentioned key climate variables, an evident signal related to the season and elevation of occurrence and to the type of process and size of the event, emerges. More specifically, the role of precipitation decreases (and that of temperature increases) from spring (41%) to winter (0%), and from the low (42%) to the high (5%) elevations. Debris/mudflow occurrence is well related to precipitation anomalies (47%) compared to landslides (27%), but, surprisingly, the same percentage (25%) of debris/mudflows and landslides occur in association to positive temperature anomalies. Finally, small-volume events are better explained by the four key selected climate variables than large events; however, these latter appear to be much more sensitive to temperature anomalies (33%) than to precipitation (4%).

The high occurrence of positive temperature anomalies in the lead-up of a failure, associated or not with heavy precipitation, supports the hypothesis of a role of climate warming in the occurrence of mass-wasting processes at high-elevation sites in recent years. This evidence is also confirmed by the different distribution of temperature and precipitation

anomalies across season and elevation of occurrence. According to past climate trends and future projections, we can expect that, for the Italian Alps, slope instability driven by positive temperature anomalies will become more and more important, while processes related to long-term precipitations will lose relevance.

In conclusion, the statistical approach proposed here represents a standardized method, which can be applied to different contexts, implemented with additional variables (e.g., solar radiance) and used to compare climate change impact on different natural processes. In the field of geohazards, the interpretation of the mechanisms leading to slope failure in the light of the main climate anomalies detected represents a challenging avenue for future research and an essential step for the knowledge and management of global warming impacts.

Acknowledgements This research was conducted with funding provided by CNR IRPI Torino. Francesco Laio acknowledges funding from the ERC grant #647473. The Authors thank ARPA Piemonte, ARPA Lombardia, ARPA Veneto, Centro Funzionale - Regione Autonoma Valle d'Aosta, Ufficio Idrografico - Provincia Autonoma di Bolzano, Meteorentino, and ARPA FVG for providing access to their databases of climate records. The Authors thank the IRPI personnel and external collaborators who, over time, contributed to the collection and organization of the documentation on slope instability, in particular: Dr. Matteo Collimedaglia (naturalist of the CNR IRPI Torino), Dr. Fabrizio Kranitz (Regione Friuli-Venezia Giulia), Dr. Paolo Fassi (Regione Lombardia-Servizio Tecnico Sala Operativa), Dr. Luciano Arziliero (Regione Veneto), and Dr. Volkmar Mair (Provincia autonoma di Bolzano – Alto Adige).

Publisher's note Springer Nature remains neutral with regard to jurisdictional claims in published maps and institutional affiliations.

References

- Allen S, Huggel C (2013) Extremely warm temperatures as a potential cause of recent high mountain rockfall. *Glob Planet Chang* 107:59–69
- ARPA Lombardia (2018) ARPA Lombardia. <http://www.arpalombardia.it/siti/arpalombardia/meteo/osservazioniedati/datitemporeale/rilevazioni-in-tempo-reale/Pagine/Rilevazioni-in-tempo-reale.aspx>. Accessed 29 Jan 2018
- ARPA Piemonte (2018a) Banca Dati Eventi del Piemonte. http://webgis.arpa.piemonte.it/Geoviewer2D/index.html?config=other-configs/bde_config.json. Accessed 2 March 2018
- ARPA Piemonte (2018b) Accesso ai dati » Annali meteorologici ed idrologici » Banca dati meteorologica. https://www.arpa.piemonte.gov.it/rischinaturali/accesso-ai-dati/annali_meteoidrologici/annali-meteo-idro/banca-dati-meteorologica.html. Accessed 29 Jan 2018
- ARPAV (2018) ARPAV. http://www.arpa.veneto.it/bollettini/meteo60gg/Mappa_TEMP.htm. Accessed 29 Jan 2018
- Auer I, Bohm R, Jurkovic A et al (2007) HISTALP - historical instrumental climatological surface time series of the Greater Alpine Region. *Int J Climatol* 27:17–46. <https://doi.org/10.1002/joc.1377>
- Avanzi F, De Michele C, Gabriele S et al (2015) Orographic signature on extreme precipitation of short durations. *J Hydrometeorol* 16:278–294. <https://doi.org/10.1175/JHM-D-14-0063.1>

- Dal Piaz G, Bistacchi A, Massironi M (2003) Geological outline of the Alps. *Episodes* 26:175–180
- Beniston M, Farinotti D, Stoffel M, Andreassen LM, Coppola E, Eckert N, ..., Huwald H (2018) The European mountain cryosphere: a review of its current state, trends, and future challenges. *Cryosphere* 12(2):759–794
- Brunetti M, Lentini G, Maugeri M, Nanni T, Auer I, Boehm R, Schoener W (2009) Climate variability and change in the greater alpine region over the last two centuries based on multi-variable analysis. *Int J Climatol* 29:2197–2225. <https://doi.org/10.1002/joc.1857>
- Buisan ST, López-Moreno JI, Saz MA, Kochendorfer J (2016) Impact of weather type variability on winter precipitation, temperature and annual snowpack in the Spanish Pyrenees. *Clim Res* 69(1):79–92
- Cardinali M, Ardizzone F, Galli M et al (2000) Landslides triggered by rapid snow melting: the December 1996-January 1997 event in Central Italy. *Proceedings of the EGS Plinius Conference*, Editoriale Bios, Cosenza, Maratea, Italy, pp 439–448
- Centro Funzionale Valle D'Aosta (2018) Meteo CF VDA - Stazioni meteo. http://cf.regione.vda.it/lista_stazioni.php. Accessed 29 Jan 2018
- Chadburn SE, Burke EJ, Cox PM, Friedlingstein P, Hugelius G, Westermann S (2017) An observation-based constraint on permafrost loss as a function of global warming. *Nat Clim Chang* 7:340–344. <https://doi.org/10.1038/nclimate3262>
- Chiarle M, Geertsema M, Mortara G, Clague JJ (2011) Impacts of climate change on debris flow occurrence in the cordillera of Western Canada and the European Alps. In: Genevois R, Hamilton DL, Prestininzi A (eds) *Proceedings of the 5th International Conference on Debris-Flow Hazards Mitigation, Mechanics, Prediction and Assessment*, Padua, Italy - 14-17 June 2011. Università La Sapienza, Roma, pp 45–52
- Collins BD, Stock GM (2016) Rockfall triggering by cyclic thermal stressing of exfoliation fractures. *Nat Geosci* 9:395–400. <https://doi.org/10.1038/ngeo2686>
- Cremonese E, Gruber S, Phillips M, Pogliotti P, Boeckli L, Noetzli J, Suter C, Bodin X, Crepez A, Kellerer-Pirklbauer A, Lang K, Letey S, Mair V, Morra di Cella U, Ravel L, Scapozza C, Seppi R, Zischg A (2011) An inventory of permafrost evidence for the European Alps. *Cryosph* 5:651–657. <https://doi.org/10.5194/tc-5-651-2011>
- Crespi A, Brunetti M, Lentini G, Maugeri M (2017) 1961-1990 high-resolution monthly precipitation climatologies for Italy. *Int J Climatol* 38:878–895. <https://doi.org/10.1002/joc.5217>
- Crozier MJ (2010) Deciphering the effect of climate change on landslide activity: a review. *Geomorphology* 124(3–4):260–267
- Davies MCR, Hamza O, Harris C (2001) The effect of rise in mean annual temperature on the stability of rock slopes containing ice-filled discontinuities. *Permafrost Periglacial Process* 12:137–144. <https://doi.org/10.1002/ppp.378>
- Dehn M, Bürger G, Buma J, Gasparetto P (2000) Impact of climate change on slope stability using expanded downscaling. *Eng Geol* 55(3):193–204
- Deline P et al (2015) Chapter 15 - Ice Loss and Slope Stability in High-Mountain Regions. In: Shroder JF, Haeberli W, Whiteman C (eds) *Snow and Ice-Related Hazards, Risks and Disasters*. Academic Press, pp 521–561
- Esposito S, Alilla R, Beltrano MC, Dal Monte G, Di Giuseppe E, Iafrate L, Libertà A, Parisse B, Raparelli E, Scaglione M (2014) *Atlante italiano del clima e dei cambiamenti climatici, Progetto Agrosenari, Consiglio per la Ricerca e la Sperimentazione in Agricoltura, Unità di Ricerca per la Climatologia e la Meteorologia applicate all'Agricoltura*, 29–30 October 2014, Rome, Italy
- Fischer L, Kääh A, Huggel C, Noetzli J (2006) Geology, glacier retreat and permafrost degradation as controlling factors of slope instabilities in a high-mountain rock wall: the Monte Rosa east face. *Nat Hazards Earth Syst Sci* 6:761–772
- Fischer L, Purves RS, Huggel C, Noetzli J, Haeberli W (2012) On the influence of topographic, geological and cryospheric factors on rock avalanches and rockfalls in high-mountain areas. *Nat Hazards Earth Syst Sci* 12:241–254. <https://doi.org/10.5194/nhess-12-241-2012>
- GAPHAZ (2017) *Assessment of Glacier and Permafrost Hazards in Mountain Regions – Technical Guidance Document*. Prepared by Allen S, Frey H, Huggel C et al. Standing Group on Glacier and Permafrost Hazards in Mountains (GAPHAZ) of the International Association of Cryospheric Sciences (IACS) and the International Permafrost Association (IPA). Zurich, Switzerland / Lima, Peru, 72 pp
- Gariano SL, Guzzetti F (2016) Landslides in a changing climate. *Earth-Sci Rev* 162:227–252. <https://doi.org/10.1016/j.earscirev.2016.08.011>
- Geertsema M, Chiarle M (2013) Mass movement causes: glacier thinning. In: Shroder J, Marston RA, Stoffel M (eds) *Treatise on geomorphology, Mountain and Hillslope Geomorphology*, vol 7. Academic, San Diego, pp 217–222.
- Geertsema M, Clague JJ, Schwab JW, Evans SG (2006) An overview of recent large catastrophic landslides in northern British Columbia, Canada. *Eng Geol* 83(1–3):120–143
- Geertsema M, van Hees M, Chiarle M, Hayek J. (2014) Debris flow on a seasonally frozen rupture surface at Moose Lake, British Columbia. In: Shan W, Guo Y, Wang F, Marui H, Strom A (eds) *Landslides in cold regions in the context of climate change*. Environmental Science and Engineering. Springer, Cham
- Gobiet A, Kotlarski S, Beniston M, Heinrich G, Rajczak J, Stoffel M (2014) 21st century climate change in the European Alps—a review. *Sci Total Environ* 493:1138–1151. <https://doi.org/10.1016/j.scitotenv.2013.07.050>
- Gruber S, Haeberli W (2007) Permafrost in steep bedrock slopes and its temperature-related destabilization following climate change. *J Geophys Res* 112(F2)
- Haeberli W, Whiteman C, Shroder JF (eds) (2015) *Snow and Ice-Related Hazards, Risks and Disasters*. Waltham, MA: Academic Press
- Harris C, Arenson LU, Christiansen HH, Eitzelmüller B, Frauenfelder R, Gruber S, Haeberli W, Hauck C, Hölzle M, Humlum O, Isaksen K, Kääh A, Kern-Lütschg MA, Lehning M, Matsuoka N, Murton JB, Nötzli J, Phillips M, Ross N, Seppälä M, Springman SM, Vonder Mühl D (2009) Permafrost and climate in Europe: monitoring and modelling thermal, geomorphological and geotechnical responses. *Earth-Sci Rev* 92:117–171. <https://doi.org/10.1016/j.earscirev.2008.12.002>
- Hasler A, Gruber S, Beutel J (2012) Kinematics of steep bedrock permafrost. *J Geophys Res* 117: F01016. <https://doi.org/10.1029/2011JF001981>
- HISTALP (2018) HISTALP. <http://www.zamg.ac.at/histalp/>. Accessed 26 Jan 2018
- Huggel C, Salzmann N, Allen S, Caplan-Auerbach J, Fischer L, Haeberli W, Larsen C, Schneider D, Wessels R (2010) Recent and future warm extreme events and high-mountain slope stability. *Philos Trans A Math Phys Eng Sci* 368:2435–2459. <https://doi.org/10.1098/rsta.2010.0078>
- Huggel C, Allen S, Clague JJ, Fischer L, Korup O, Schneider D (2013) Detecting potential climate signals in large slope failures in cold mountain regions. In: *Landslide science and practice*. Springer Berlin Heidelberg, Berlin, Heidelberg, pp 361–367
- Isotta FA, Frei C, Weigluni V, Perčec Tadić M, Lassègues P, Rudolf B, Pavan V, Cacciamani C, Antolini G, Ratto SM, Munari M, Micheletti S, Bonati V, Lussana C, Ronchi C, Panettieri E, Marigo G, Vertačnik G (2014) The climate of daily precipitation in the Alps: development and analysis of a high-resolution grid dataset from pan-Alpine rain-gauge data. *Int J Climatol* 34:1657–1675. <https://doi.org/10.1002/joc.3794>

- Jakob M, Lambert S (2009) Climate change effects on landslides along the southwest coast of British Columbia. *Geomorphology* 107(3–4): 275–284
- Jakob M, Owen T, Simpson T (2012) A regional real-time debris-flow warning system for the District of North Vancouver, Canada. *Landslides* 9(2):165–178
- Kääb A, Chiarle M, Raup B, Schneider C (2007) Climate change impacts on mountain glaciers and permafrost. *Glob Planet Chang* 56:vii–ix
- Luino F (2005) Sequence of instability processes triggered by heavy rainfall in northwestern Italy. *Geomorphology* 66:13–39
- Luino F, Turconi L (2017) Eventi di piena e frana in Italia settentrionale nel periodo 2005–2016. Ed. SMI, ISBN 978-88-903023-8-1
- Ma T, Li C, Lu Z, Wang B (2014) An effective antecedent precipitation model derived from the power-law relationship between landslide occurrence and rainfall level. *Geomorphology* 216:187–192
- Magnin F, Deline P, Ravanel L, Noetzi J, Pogliotti P (2015) Thermal characteristics of permafrost in the steep alpine rock walls of the Aiguille du Midi (Mont Blanc Massif, 3842 m asl). *Cryosphere* 9(1):109–121
- Merlone A, Lopardo G, Sanna F, Bell S, Benyon R, Bergerud RA, Bertiglia F, Bojkovski J, Böse N, Brunet M, Cappella A, Coppa G, del Campo D, Dobre M, Drnovsek J, Ebert V, Emardson R, Fernicola V, Flakiewicz K, Gardiner T, Garcia-Izquierdo C, Georgin E, Gilbert A, Grykalowska A, Grudniewicz E, Heinonen M, Holmsten M, Hudoklin D, Johansson J, Kajastie H, Kaykızılı H, Klason P, Kňazovická L, Lakka A, Kowal A, Müller H, Musacchio C, Nwaboh J, Pavlasek P, Piccato A, Pitre L, de Podesta M, Rasmussen MK, Sairanen H, Smorgon D, Sparasci F, Strnad R, Szymrka-Grzebyk A, Underwood R (2015) The MeteoMet project - metrology for meteorology: challenges and results. *Meteorol Appl* 22:820–829. <https://doi.org/10.1002/met.1528>
- Meteotrentino (2018) Meteotrentino. <https://www.meteotrentino.it/?id=168#!/content?menuItemDesktop=111>. Accessed 29 Jan 2018
- Mountain Research Initiative EDW Working Group (2015) Elevation-dependent warming in mountain regions of the world. *Nat Clim Chang* 5:424–430. <https://doi.org/10.1038/nclimate2563>
<http://www.nature.com/nclimate/journal/v5/n5/abs/nclimate2563.html#supplementary-information>
- Nigrelli G, Fratianni S, Zampollo A, Turconi L, and Chiarle M (2018) The altitudinal temperature lapse rates applied to high elevation rockfalls studies in the Western European Alps. *Theor Appl Climatol* 131(3–4):1479–1491
- Nigrelli G, Lucchesi S, Bertotto S, Fioraso G, Chiarle M (2014) Climate variability and Alpine glaciers evolution in Northwestern Italy from the Little Ice Age to the 2010s. *Theor Appl Climatol* 122:595–608. <https://doi.org/10.1007/s00704-014-1313-x>
- Northon K (2017) NASA, NOAA data show 2016 warmest year on record globally. <https://www.nasa.gov/press-release/nasa-noaa-data-show-2016-warmest-year-on-record-globally>. Accessed 29 Jan 2018
- Palladino MR, Viero A, Turconi L, Brunetti MT, Peruccacci S, Melillo M, Luino F, Deganutti AM, Guzzetti F (2018) Rainfall thresholds for the activation of shallow landslides in the Italian Alps: the role of environmental conditioning factors. *Geomorphology* 303:53–67. <https://doi.org/10.1016/J.GEOMORPH.2017.11.009>
- Paranunzio R, Laio F, Nigrelli G, Chiarle M (2015) A method to reveal climatic variables triggering slope failures at high elevation. *Nat Hazards* 76:1039–1061. <https://doi.org/10.1007/s11069-014-1532-6>
- Paranunzio R, Laio F, Chiarle M, Nigrelli G, Guzzetti F (2016) Climate anomalies associated with the occurrence of rockfalls at high-elevation in the Italian Alps. *Nat Hazards Earth Syst Sci* 16:2085–2106. <https://doi.org/10.5194/nhess-16-2085-2016>
- Paranunzio R, Chiarle M, Laio F et al (2017) Climatic conditions associated to the occurrence of slope instabilities in the Italian Alps in year 2016. *EGU Gen Assem Conf Abstr* 19:13227
- Pavlova I, Jomelli V, Brunstein D, Grancher D, Martin E, Déqué M (2014) Debris flow activity related to recent climate conditions in the French Alps: a regional investigation. *Geomorphology* 219:248–259. <https://doi.org/10.1016/J.GEOMORPH.2014.04.025>
- Pepin N, Bradley RS, Diaz HF et al. (2015) Elevation-dependent warming in mountain regions of the world. *Nat Clim Chang* 5(5): 424–430. <https://doi.org/10.1038/NCLIMATE2563>
- Peruccacci S, Brunetti MT, Gariano SL, Melillo M, Rossi M, Guzzetti F (2017) Rainfall thresholds for possible landslide occurrence in Italy. *Geomorphology* 290:39–57. <https://doi.org/10.1016/J.GEOMORPH.2017.03.031>
- Protezione Civile - Provincia Autonoma di Trento (2018) Primo Piano - Prevenzione e Territorio. http://www.protezionecivile.tn.it/territorio/primop_territorio/. Accessed 2 March 2018
- Provincia autonoma di Bolzano - Alto Adige (2018). <http://meteo.provincia.bz.it/>. Accessed 29 Jan 2018
- Ravanel L, Deline P (2015) Rockfall hazard in the Mont Blanc Massif increased by the current atmospheric warming. In: *Engineering geology for society and territory - volume 1*. Springer International Publishing, Cham, pp 425–428
- Ravanel L, Magnin F, Deline P (2017) Impacts of the 2003 and 2015 summer heatwaves on permafrost-affected rock-walls in the Mont Blanc massif. *Sci Total Environ* 609:132–143. <https://doi.org/10.1016/J.SCITOTENV.2017.07.055>
- RAVdA (2018) Catasto Dissesti Regionale - SCT. <http://catastodissesti.partout.it/>. Accessed 2 March 2018
- Rebetez M, Lugon R, Baeriswyl PA (1997) Climatic change and debris flows in high mountain regions: the case study of the Ritigraben Torrent (Swiss Alps). In: *Climatic change at high elevation sites*. Springer Netherlands, Dordrecht, pp 139–157
- Saez JL, Corona C, Stoffel M, Berger F (2013) Climate change increases frequency of shallow spring landslides in the French Alps. *Geology* 41:619–622. <https://doi.org/10.1130/G34098.1>
- Salvatore MC, Zanoner T, Baroni C, Carton A, Banchieri FA, Viani C, Giardino M, Perotti L (2015) The state of Italian glaciers: a snapshot of the 2006–2007 hydrological period. *Geogr Fis Din Quat* 38:175–198 2015
- Schar C, Vidale PL, Luthi D et al (2004) The role of increasing temperature variability in European summer heatwaves. *Nature* 427:332–336. <https://doi.org/10.1038/nature02300>
- SINAnet Ispra (2017) DEM20 — Italiano. <http://www.sinanet.isprambiente.it/it/sia-ispra/download-mais/dem20/view>. Accessed 29 Jan 2018
- Smiraglia C, Azzoni RS, D'agata C et al (2015) The evolution of the Italian glaciers from the previous data base to the new Italian inventory. Preliminary considerations and results. *Geogr Fis Din Quat* 38: 79–87. <https://doi.org/10.4461/GFDQ.2015.38.08>
- Stocker TF, Qin D, Plattner GK et al (2013) IPCC, 2013: climate change 2013: the physical science basis. Contribution of working group I to the fifth assessment report of the intergovernmental panel on climate change. IPCC AR5:1535
- Stoffel M, Huggel C (2017) Mass movements in periglacial environments. In: *International encyclopedia of geography: people, the earth, environment and technology*. John Wiley & Sons, Ltd, Chichester, pp 1–8
- Stoffel M, Bollschweiler M, Beniston M (2011) Rainfall characteristics for periglacial debris flows in the Swiss Alps: past incidences–potential future evolutions. *Clim Chang* 105(1–2):263–280
- Team CW, Pachauri RK, Meyer LA (2014) IPCC Climate Change 2014: Synthesis Report Summary for Policymakers. Contribution of Working Groups I, II and III to the Fifth Assessment Report of the Intergovernmental Panel on Climate Change
- Trigila A, Iadanza C, Spizzichino D (2010) Quality assessment of the Italian landslide inventory using GIS processing. *Landslides* 7: 455–470. <https://doi.org/10.1007/s10346-010-0213-0>

- Turconi L, Kumar De S, Tropeano D, Savio G (2010) Slope failure and related processes in the Mt. Rocciamelone area (Cenischia Valley, Western Italian Alps). *Geomorphology* 114:115–128. <https://doi.org/10.1016/j.geomorph.2009.06.012>
- Weber S, Beutel J, Faillettaz J, Hasler A, Krautblatter M, Vieli A (2017) Quantifying irreversible movement in steep, fractured bedrock permafrost on Matterhorn (CH). *Cryosphere* 11:567–583. <https://doi.org/10.5194/tc-11-567-2017>
- Wieczorek GF, Glade T (2005) Climatic factors influencing occurrence of debris flows. In: Jakob M, Hungr O (eds) *Debris flow hazards and related phenomena*. Springer, Berlin, pp 325–362
- Zemp M, Frey H, Gärtner-Roer I, Nussbaumer SU, Hoelzle M, Paul F, Haeblerli W, Denzinger F, Ahlstrøm AP, Anderson B, Bajracharya S, Baroni C, Braun LN, Cáceres BE, Casassa G, Cobos G, Dávila LR, Delgado Granados H, Demuth MN, Espizua L, Fischer A, Fujita K, Gadek B, Ghazanfar A, Ove Hagen J, Holmlund P, Karimi N, Li Z, Pelto M, Pitte P, Popovnin VV, Portocarrero CA, Prinz R, Sangewar CV, Severskiy I, Sigurdsson O, Soruco A, Usabaliev R, Vincent C (2015) Historically unprecedented global glacier decline in the early 21st century. *J Glaciol* 61:745–762. <https://doi.org/10.3189/2015JG15J017>